Islam, A H M Mainul, M.A. December 2021 Geography

TRACKING CYCLONIC (SIDR) IMPACT AND RECOVERY RATE OF MANGROVE FOREST USING REMOTE SENSING: A CASE STUDY OF THE SUNDARBANS, BANGLADESH

Thesis Advisor: Timothy Assal

ABSTRACT

The Sundarbans mangrove forest, one of the world's largest of its kind situated at the southwest of Bangladesh (approximately 60%), plays a vital role in safeguarding the country from the wrath of tropical cyclones and other disaster events. It is known to act as a vegetative shield to protect cyclonic wind's initial threat during any tropical cyclone towards Bangladesh. During Sidr (November 15, 2007), the second-largest cyclone in Bangladesh since 1877, it is estimated that the Sundarbans lost 30% of its plant habitat while upwards of 15% of the forest sustained severe damage. To manage the natural resources of the Sundarbans after disturbance, proper study regarding the impact and post-disturbance recovery of the forests is an immediate requirement. Most of the literature has focused on change in land cover types, which can help investigate the overall impact. However, the question of how long it takes these forests to recover is still relatively unexplored. This study used a pixel-based approach using MODIS (MOD09Q1.006 Terra Surface Reflectance 8-Day Global 250m product) to explore the impact of Sidr and further recovery of the Sundarbans. State QA Bitmask was used to mask out the clouds, cloud shadows, and water from the images using Google Earth Engine (GEE) to ensure the quality of pixels. A specific threshold level was determined to collect the clear sky

observations only. Plant productivity anomalies were used to understand the change in vegetation condition related to cyclone Sidr. Season based impact analysis was performed using a known reference period to determine the deviation from normal growth condition. I found that the east side of the Sundarbans's was severely impacted, with a total of 2,261 sq. km. (approx.) being negatively impacted during the dry season immediately after Sidr. This area of the Sundarbans took approximately 3 years (2007 to 2010) to recover from the damage. This study is reproducible and rapid assessment for cyclone impact on the Sundarbans based on the availability of clear sky observations.

TRACKING CYCLONIC (SIDR) IMPACT AND RECOVERY RATE OF MANGROVE FOREST USING REMOTE SENSING: A CASE STUDY OF THE SUNDARBANS, BANGLADESH

A thesis submitted

To Kent State University in partial

Fulfillment of the requirements for the

Degree of Master of Arts

By

A H M Mainul Islam

December 2021

Thesis written by

A H M Mainul Islam

BURP, Khulna University of Engineering & Technology, 2016

M.A., Kent State University, 2021

Approved by

Dr. Timothy Assal, Advisor

Dr. Scott Sheridan, Chair, Department of Geography

Dr. Mandy Munro-Stasiuk, Interim Dean, College of Arts and Sciences

TABLE OF CONTENTS

LIST OF FIGURES

LIST OF TABLES

ACKNOWLEDGEMENTS

I would like to express my utmost gratitude and respect to my thesis advisor, Dr. Timothy Assal for his continuous motivation, timely guidance, constructive criticism, and important suggestions during my thesis work. His expertise in landscape dynamics monitoring has motivated me to pursue research in mangrove ecosystem dynamics. Without his help and support, I would not be able to overcome the difficulties I faced during my two and half year's journey at Kent State University (KSU).

I would like to thank the Department of Geography at Kent State University (KSU) for this opportunity and the funding assistance to complete my degree.

I would also like to thank my committee members, Dr. Emariana Widner, and Dr. He Yin for their helpful suggestions and discussions which made me think more logically to finish the thesis.

I am extremely thankful to the Biogeography and Landscape Dynamics Lab at KSU and my amazing lab members- Nicholas Manning, Michelle Escalambre, and Hana Matsumoto for their constant support and encouragement during the research.

I would like to specially mention my colleague Nicholas Manning who helped me immensely to develop the Google Earth Engine codes. I am deeply grateful to him for his effective guidance and suggestions regarding the codes and remote sensing strategies.

Finally, my sincere gratitude goes to my family members and to all my friends in Bangladesh for their love and involvement in my past two and half years residing in the United States. I successfully overcame all hurdles here due to their continuous support.

CHAPTER 1: INTRODUCTION

1.1 The big picture

The Sundarbans [1] is a deltaic mangrove forest and is considered a globally unique ecosystem (Aziz & Paul, 2015). It is recognized as the largest, continuous mangrove forest in the world that lies in the vast delta of Bay of Bengal (Akber et al., 2018; Dutta et al., 2015). It is shared between Bangladesh (60%) and India (40%) (Quader et al., 2017). The Bangladesh side of the Sundarbans occupies 4.2% (6197 km^2) of the total area of country's land area (147,570 km^2) and constitutes 44% (6276 km^2) of the forest cover in the country (14,264 km^2). As Bangladesh is a cyclone prone country, at least 54 cyclones made landfall from the Bay of Bengal between 1977 to 2010 (at least 12 after 2000). Approximately 2500 $km^2$of the total area of the Sundarbans mangrove forest was impaired by cyclone Sidr, 2007.

The Sundarbans provides coastal safety to millions of people in Bangladesh and India (Giri et al., 2007), and acts as a vegetative shield in the direction of storm surges that helps to minimize adverse impacts. Cyclone Sidr, a category-4 equivalent tropical cyclone, made landfall in Bangladesh on November 15, 2007, with a recorded wind speed of 132 miles per hour. UNESCO estimated Sidr damaged over 40% of the Sundarbans. Previous research has focused on long-term changes in forest cover, land cover, and land use of mangrove forest area to conduct study yet little research has focused on the Sundarbans forest condition and recovery from cyclones. I

[1] The terms "The Sundarbans" and "The Sundarban" are interchangeably used in different literature. Most studies used "the Sundarbans" if the study area considered both Indian and Bangladesh side of the mangrove forest while some of the studies considered using "the Sundarban" if the study area is only in Bangladesh or India. Few studies based on Bangladesh side forest also used "the Sundarbans". For this study, I am using "the Sundarbans" to define my study area.

used a remote sensing time-series analysis to address the extent and severity of the cyclone in Sundarbans on vegetation condition from its pre-disturbance condition. Given the high frequency of cyclones, the impact of these events on vegetation condition of the Sundarbans is an important research need. It is important to know about the extent and severity of damage and recovery of ecosystem after disturbance to prepare accordingly for next disturbance event. Recovery rate and pattern can be a useful addition to disaster management for forest ecosystems. However, proper monitoring is necessary to determine these characteristics.

1.2 Mangrove Ecology

Mangroves are widely distributed in the regions between 30° north and south of the equator. The area extends to the north in Bermuda (32° 20'N) and Japan (31° 22'N), and to the south in Australia (38° 45'S), New Zealand (38° 03'S) and the east coast of South Africa (32° 59'S) (Spalding et al., 1997). Some of the most extensive mangrove forests are found in the Sundarbans, Mekong Delta, Amazon, Madagascar, Papua New Guinea and Southeast Asia (Giri et al., 2011). These regions are known as tropical and sub-tropical and have favorable climate for mangrove ecosystems (Kanniah et al., 2015). Mangroves can be seen along the coast side of these regions as a link between land and water (Islam et al., 2019). Globally, there are approximately 137,760 km^2 of mangrove forests in the tropical and sub-tropical regions of the world (Giri et al., 2011) (Table 1).

Table 1: Global Percentage Distribution of Mangrove, based on 2011 estimate by C. Giri et al. (2011)

Region	**Area in km^2**	**Global percentage**
Asia	57859.2	42
Africa	27552	20
North & Central America	20664	15
Oceania	16531.2	12
South America	15153.6	11

This ecosystem is colonized by a unique botanical cluster of woody plants which adapted to the coastal areas where fresh water and saline water meet (Islam et al., 2019). Mangrove plants are highly adapted to the hostile environment of the sea caused by high salinity, wave activities, and vacillating water levels (Hogarth, 2015). Mangroves are salt-tolerant evergreen plants that grow in intertidal marine zones with a number of distinctive growth patterns (T. Wang et al., 2016). A specific feature of all mangrove species is an aboveground root system which enables the plants to exchange oxygen, which is limited in the saturated soil. Mangroves developed a process to maintain nutrient retention and reproduction through pre-leaf fall nutrient reabsorption, and limiting nutrient movement in leaf litter during decomposition (Reef et al., 2010). Lacking an understory makes the mangroves different from the tropical terrestrial forests (Janzen, 1985). Mangroves also contain specialized mechanisms for viviparous embryos and tidal dispersal of propagules. Due to geographic specifics mangrove trees only grow within tropical and subtropical latitudes and there are 9 orders, 20 families, 27 genera, and roughly 70 species of mangrove (Alongi, 2009). According to Alongi (2009), the Indo-West Pacific region is the most diverse region for mangrove species (Figure 1). Mangrove trees are limited globally by

temperature and their extent is determined by variations in rainfall, tides, waves, and river flow greatly at the regional and local scale.

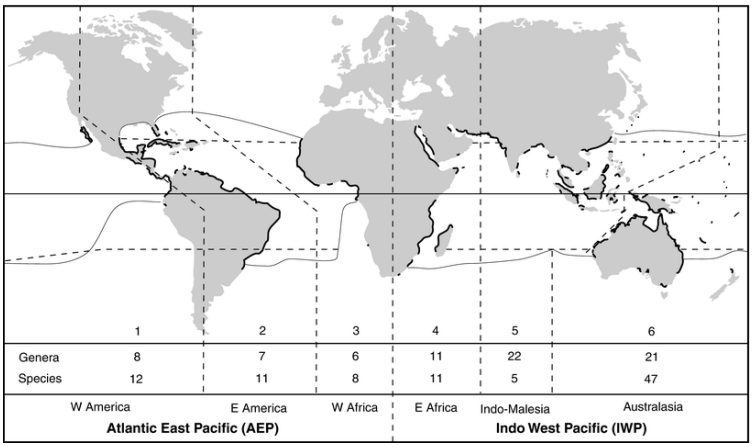

Figure 1: Global distribution of the world's mangrove forests and their biogeographic provinces. Number of genera and species within each province are noted below the map. (Hogarth, 2015)

Mangroves form one of the most productive ecosystems in the world, delivering nutrients and organic matter to adjacent coastal environments and anchoring a complex food web (Alongi, 2009). Mangroves are also very valuable to humans, providing numerous ecosystem services, whereas storm damage buffering is considered one of the most important (Das & Vincent, 2009; Marois & Mitsch, 2015; Akber et al., 2018; Sandilyan & Kathiresan, 2015). Mangroves only constitute 0.4% of the world's total forest composition, yet provide valuable carbon capture and storage (Kanniah et al., 2015), and protect coastal areas from the impacts storm surges (Das & Crépin, 2013). They neutralized the severity of the Boxing Day tsunami in 2004 toward the northern tip of Sumatra in Indonesia. This is an example of the capability of mangroves to check the surge impact in the inward side of the forest and attenuate the wind and waves in coastal areas (Das & Crépin, 2013). Several studies on this tsunami reported greater damage in villages that did not have mangrove forests acting as bio-shield compared to villages with intact mangrove forests (Danielsen et al., 2005; Kathiresan & Rajendran, 2005; Das & Vincent, 2009).

A super cyclone in Odisha, landed in 1999, killed almost 10,000 and caused heavy damage to livestock and property in several coastal villages without mangrove belts. It was estimated that 90% of the damages could have been avoided if there was intact mangrove forests (Sandilyan & Kathiresan, 2015; Das & Vincent, 2009). Thirty trees per $100m^2$ in a 100m wide coastal forest belt can limit the flow pressure of a tsunami by more than 90% (Hiraishi & Harada, 2003). Several other studies demonstrated that a 6-year-old mangrove forest of 1.5km width can attenuate the speed of 1m high waves at the open sea and 0.05m at the coast (Mazda et al., 1997; Kathiresan & Rajendran, 2005). Therefore, the role of mangroves as a bio-shield is undeniable and well-established (Sandilyan & Kathiresan, 2012; Das & Vincent, 2009; Dasgupta et al., 2017; Marois & Mitsch, 2015; Sanford, 2009; Akber et al., 2018). According to Barbier et al. (2008), the buffering capability of mangroves during tsunamis and tropical storms has been underrated, but the importance of valuating coastal protection by mangrove ecosystems has gained a lot of attention in recent decades (Sanford, 2009).

1.3 The Sundarbans Mangrove Forest

The Sundarbans mangrove forest is the largest continuous area of mangroves in the world and covers an area of approximately 10,000 sq. km. (Giri et al., 2015; Spalding et al., 1997; Bhowmik & Cabral, 2011), with approx.. 60% located in Bangladesh (Dutta et al., 2015). It is in the south-west of Bangladesh (Figure 2) between the river Baleswar in the East and the Harinbanga in the West, adjoining to the Bay of Bengal (Aziz & Paul, 2015) . The forest covers an area of 6,017 sq. km. (4.2% of the total area of Bangladesh), constitutes 44% of the forest cover in the country, and contains 65 mangrove species (Aziz & Paul, 2015). It lies in a zone facing cyclonic storms and provides coastal protection to millions of people in Bangladesh by limiting storm surge height through tree roots, trunks, and leaves that together obstruct the flow

of water (Deb & Ferreira, 2017). Mangrove species, density, and forest structure are important factors which influence the performance of mangrove forests in wave energy dissipation. Effective management is needed to maximize protection to coastal communities, which requires location-specific data on mangrove ecosystems (Dasgupta et al., 2019).

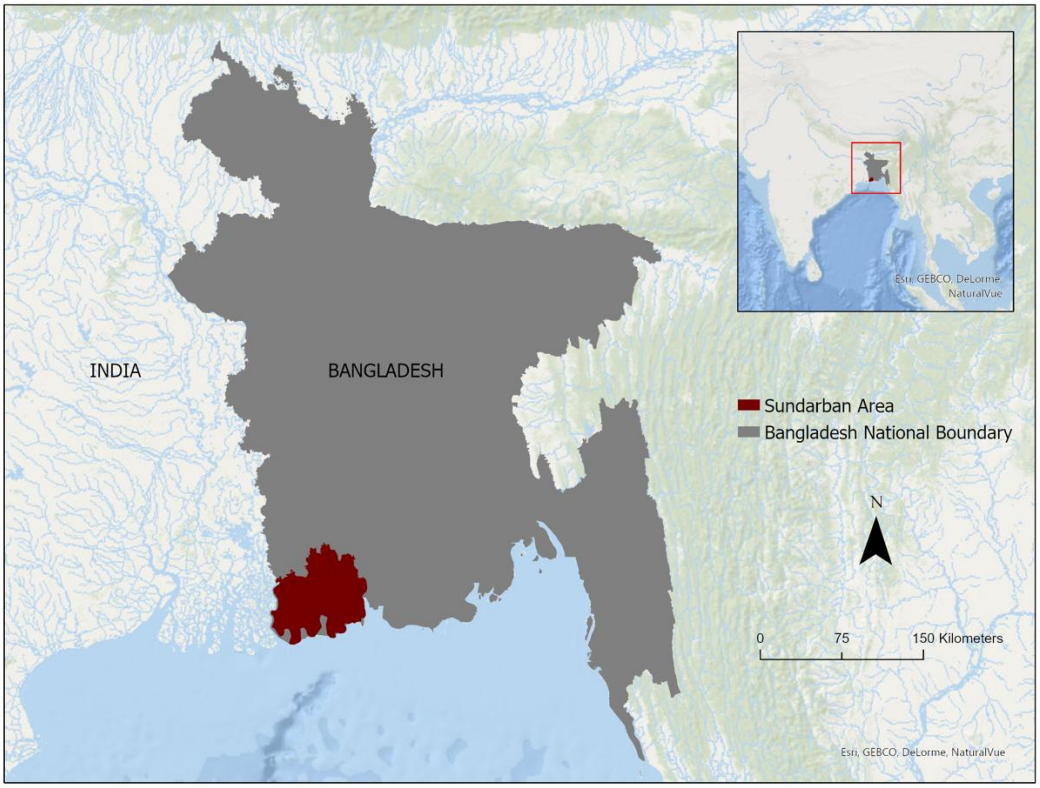

Figure 2: Location map of the Sundarbans (Bangladesh part) (Data Source: ESRI base map and the author)

Sundari (*Heritiera fomes*) is the most influential and tallest (over 15m) plant in the Sundarbans (Aziz & Paul, 2015). There are several other common species in the Sundarbans such as, Passur (*Xylocarpus moluccensis*), Goran (*Ceriops roxburghiana*), Kankra (*Bruguiera gymnorhiza*), Keora (*Sonneratia apetala*) and Baen (*Avicennia officinalis*). Distribution of plants in the Sundarbans is heterogenous which are controlled by elevation and salinity. The coasts of Bangladesh represent strong monsoon-influenced tropical climate and classified the climate as

tropical moist forests (A. K. F. Hoque & Datta, 2005). The total annual rainfall increases from west to east of the coastline, and 80-85% of annual rainfall occurs during the monsoon season from May to September (Figure 3).

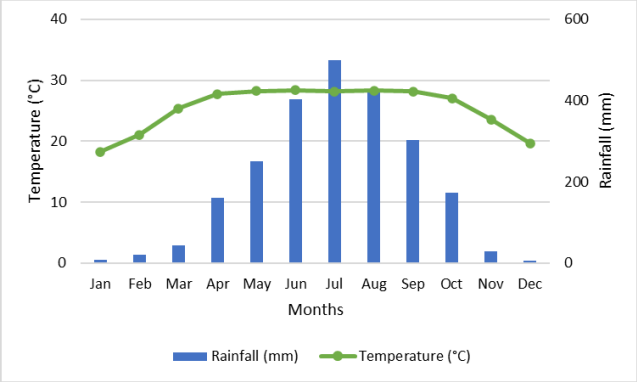

Figure 3: Average monthly temperature and rainfall in Bangladesh from 1991-2016 (adapted from World Bank Climate Data)

Changes in mangrove species composition and spatial distribution are influenced by differences in temperature and rainfall (Ghosh et al., 2017). This study found several mangrove species (*Heritiera fomes*, *Sonneratia apelatala*, and *Ceriops decandra*) showed a strong relationship with temperature and rainfall in the Sundarbans. Spatial growth of mangroves will likely be interrupted as rainfall patterns are changing globally, with a predicted increase by about 25% by 2050 (Gilman et al., 2008). Higher precipitation enhances diversity, growth and productivity while lesser rainfall increases salinity which causes competition among the mangrove species to survive (Ghosh et al., 2017). Between 1906 and 2005, average temperature has increased globally by 0.74°C and several mangrove species also show sensitivity to temperature change (Field, 1995). Mangrove phenological patterns, species composition, and productivity are expected to be impacted due to a global increase in temperature (Gilman et al., 2008; Field, 1995). The climate of the Sundarbans includes pre-monsoon, monsoon, post-monsoon, and dry winter seasons. Based on the World Bank Climate Portal data, it can be said that the rainfall and

temperature in Bangladesh are closely related. Rainfall in the Sundarbans fluctuates between 1600 mm and 2000 mm, while temperature varies between 11°C to 37°C. Cyclonic storms frequently occur during May to June and during October to November along the coast of Bangladesh.

1.4 Cyclones over Bangladesh and the Sundarbans

Historically, Bangladesh is a cyclone-prone country and most of the events have hit Bangladesh through the Sundarbans. Therefore, the Sundarbans are recognized as a buffer for this region.

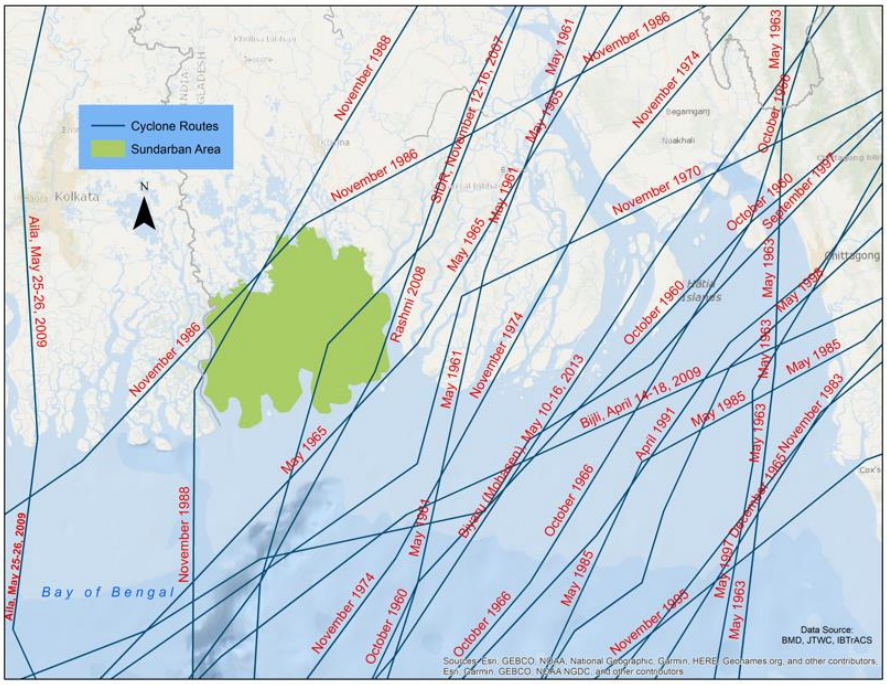

Figure 4: Cyclones over the Sundarbans and Bangladesh (historical data) (Data source: BMD, JTWC, ESRI Base map)

Most of the cyclones hit the Sundarbans first and gradually weaken before hitting land (Figure 4). As an example, approximately 2500 km^2 of the total area of the Sundarbans mangrove forest was impaired by cyclone in 2007 (Deb & Ferreira, 2017). As per the India Meteorological Department (IMD) tropical cyclone classification (depression, deep depression, cyclonic storm, severe cyclonic storm, very severe cyclonic storm), 109 cyclones hit during the pre-monsoon

period (March-April-May), compared to 421 cyclones during the post-monsoon period (October-November-December). These storm events originated in the Bay of Bengal from 1890 to 2010 (Sahoo & Bhaskaran, 2016). Cyclones and associated storm surges are the most influential disaster events in the southern coast of Bangladesh (Ahmed et al., 2016), and thus remain an important research need.

Table 2: Recent cyclones over Bangladesh (2007-2019)

Cyclone	**Year**	**Wind Speed (miles per hour)**	**Landfall**	**Source**
Akash	2007	51 mph	South of Chittagong	(Bandyopadhyay et al., 2018)
Sidr	2007	132 mph	Southern Bangladesh	
Rashmi	2008	52 mph	Southern Bangladesh	
Bijli	2009	62 mph	Chittagong and Cox's Bazar Coast	(Alam & Dominey-howes, 2015)
Aila	2009	69 mph	South-western Bangladesh	(Bandyopadhyay et al., 2018)
Viyaru	2013	52 mph	Chittagong	
Komen	2015	46 mph	Chittagong	
Roanu	2016	52 mph	Chittagong	
Mora	2017	75 mph	Chittagong	(Azad et al., 2018)
Fani	2019	62 mph	Southern Bangladesh	(Kumar et al., 2020)
Bulbul	2019	75 mph	Khulna Division	(BBC, 2019)

The southern coastal region of Bangladesh is the most tropical cyclone prone area in the country (see Figure 4). Sidr was the most devastating cyclone that overtopped the coastal area and caused huge damage to the vegetation (Bhowmik & Cabral, 2011). It was a category-4 equivalent (Saffir-Simpson Scale) tropical cyclone that made landfall in Bangladesh on November 15, 2007,

with recorded wind speeds were over 132 miles per hour and tidal waves of 6m (Bhowmik & Cabral, 2011; Ahmed et al., 2016) (Fig 4). The cyclone hit hard the eastern parts of the Sundarbans forest, especially the Chandpai range including Kochikhali, Kotka, Hiron Point, and Dublarchar (Fig 5). It was considered as the second strongest cyclone since 1877 (Aziz & Paul, 2015), and caused 10,000 deaths and $1.7 billion worth of damage (Deb & Ferreira, 2017). Biotic communities of the Sundarbans were severely affected by uprooting plants, eroding coastal soils, and breaking stems and branches of trees (Aziz & Paul, 2015).

1.5 Disturbance in the Mangroves due to Tropical Cyclones

A widely accepted definition of disturbance is a discrete event that disrupts the organizational status of an ecosystem, community, or population, and changes resource availability or the physical environment (Pickett & White, 1985). It can also be defined as a biotic or abiotic, natural or man-made process that can destabilize the natural systems at any hierarchical level (Hobbs & Huenneke, 1992). Ecological concepts such as stability, diversity, resistance, and resilience are logically linked with the concept of disturbance (Battisti et al., 2016). Disturbances are important to reshape the environment as well as the role of living organisms within it to have an impact on their evolution (Krebs, 2014). For instance, many plant communities are disturbance reliant to regenerate as many disturbance events are crucial parts of natural systems (Hobbs & Huenneke, 1992; Pickett & White, 1985). Tropical cyclones are one of the most devastating natural disturbances which can affect an ecosystem severely. The land falling tropical cyclones typically generate extreme rainfall associated with high winds and develop swell waves which can overtop coastal forest defense and cause inundation (M. A. A. Hoque et al., 2016). The global number of the most severe tropical cyclones (Category 4 and 5 on the Saffir–Simpson scale) has increased from 1975 to 2004 (Knutson et al., 2010). Cyclones often

cause vegetation defoliation, destruction of settlement/infrastructure, damage to cropland, and changes to landforms (M. A. A. Hoque et al., 2016). A change in forest structures in the cyclone path is one of the most visual post-cyclone damages due to high rate of tree mortality. Ecological disturbance induced damage have a great impact on forest biogeochemical cycles, recovery and regeneration (Krauss & Osland, 2020). In a recent review, 45% of reported mangrove mortality in the global literature were attributed to tropical cyclones (Sippo et al., 2018). Past disturbances by tropical cyclones with similar meteorological characteristics determine the type and severity of impact over the mangrove forests (Peters et al., 2011). According to Krauss & Osland (2020), tropical cyclone is a term that is mostly used in Indian Ocean and south-western Pacific Ocean while it also has other names like Hurricane and Typhoon based on locations and wind-speed. The authors focused on severity of the cyclones to call them as tropical cyclones while low-wind speed cyclones are called tropical depressions and moderate wind speed cyclones are called tropical storms. Here, I use the Saffir-Simpson scale to define the intensity of the cyclones. For instance, the Saffir-Simpson hurricane wind scale is based on speed: Category 1 (119-153 kmh^{-1}) , Category 2 (154-177 kmh^{-1}), Category 3 (178-208 kmh^{-1}), Category 4 (209-251 kmh^{-1}) and Category 5 (≥252 kmh^{-1}) (Krauss & Osland, 2020). Bangladesh, Australia, Mexico, Myanmar, Philippines, Cuba and the USA are the top regions affected by tropical cyclones (Krauss & Osland, 2020). The impact of a tropical cyclone on a mangrove forest is an important question when considering the forest recovery. A detailed description relative to Saffir-Simpson tropical cyclone intensity ratings was developed by (McAdie et al., 2009). Sidr, with a speed of 132 mph, was a category 4 cyclone according to Saffir-Simpson scale. Krauss & Osland (2020) summarized damages by Category 4 cyclone, such as massive damage of trees, including fractured crowns or blown down. Smaller trees and trees with slender trunk can be

deformed by strong wind forces. Foliage and small branches are lost, resulting in large scale cover loss, delaying the recovery of small trees. This phenomenon affects the seasonal growth phenology of surviving mangrove trees, which can extend for several seasons. Young trees and seed plants having moderate to heavy damages need to adapt to post-storm light intensity. Readjusting to the rate of light energy on per unit area is crucial for new leaf development. Satellite indices and forest structure measurements (e.g. canopy height) have been used to assess post-storm forest damages in terms of defoliation, branch loss, stem loss and other changes in forest structure (W. Wang et al., 2010). However, the number of studies on satellite remote sensing of post-storm forest damage and comparative analysis on the performances of vegetation indices are few.

1.6 Remote Sensing in Mangrove Ecosystems

Remote sensing provides a unique viewpoint on the activities happening on the Earth and plays an influential role to study intricate environmental interactions (del Río-Mena et al., 2020). Satellite remote sensing products are highly used in ecosystem research activities to quantify the interactions between vegetation and other ecosystem properties (e.g. local hydrology, energy and nutrient cycles) (Pasetto et al., 2018). Vegetation and animal population dynamics can be affected by environmental changes (Pettorelli et al., 2005): fire hazard (Szpakowski & Jensen, 2019), forest degradation (Mitchell et al., 2017), drought-induced disturbance (Assal et al., 2016), land use mapping and monitoring (Joshi et al., 2016), insect epidemic impacts (pine beetles) (Assal et al., 2014), etc. and remote sensing is the most effective tool to assess them over large areas. Remote sensing of mangroves began in the 1950s with mangrove mapping studies (Lewis & MacDonald, 1972; Everitt et al., 2008), and has since grown to include mangrove distribution mapping, biophysical parameters, and ecosystem process characterization in recent

years (L. Wang et al., 2019). The vast majority of mangrove ecology research has focused on mangrove productivity, biodiversity, and the biogeographical distribution (Finkl & Makowski, 2019). Due to the link between biological events and climate, vegetation phenology has been a focus of mangrove remote sensing research (Richardson et al., 2013; Cleland et al., 2007). Vegetation phenology is the timing of plant life cycle events, such as leaf unfolding and development, flowering, leaf senescence and litterfall (Njoku, 2014). It is an important metric to assess changes in mangrove ecosystem productivity and can be used to understand how these systems respond to climate change induced disaster events (Songsom et al., 2019). This metric is influenced by vegetation morphology, species, and microclimate variability. Phenology phases are spatially intricate and temporally dynamic and have a changing characteristic in tropical forest regions with seasonal wet/dry events. They display numerous growth periods and senescence of forests in a single annual cycle (Njoku, 2014). Traditional field methods have typically been employed to study mangrove phenology; however, these time intensive methods are not suitable to assess large landscapes. Remote sensing provides broad coverage of mangrove ecosystems at periodic time intervals (Pastor-Guzman et al., 2018). Knowledge of spatial and temporal variability from episodic disturbances is necessary to understand mangrove forest dynamics at the landscape scale and mangrove dynamics are often monitored using satellite-derived vegetation indices, such as the Normalized Difference Vegetation Index (NDVI) (Zhang et al., 2016; Long et al., 2016; Macamo et al., 2016; Kamthonkiat et al., 2011). NDVI is a measure of photosynthetic capacity of a plant canopy and considered a proxy for vegetation productivity (Rouse et al., 1974). Other indices such as EVI (enhanced vegetation index) and NMDI (normalized multi-band drought index) have also been used to monitor mangrove forests (Zhang et al., 2016; L. Wang & Qu, 2007). In order to assess the annual phenology stability

between dates, exploring different vegetation indices is useful (Assal et al., 2016). Many studies used NDVI to detect changes in vegetation condition in disturbance studies (X. Zhang et al., 2018; Wang et al., 2014; Wilson & Norman, 2018; Yang et al., 2017). NDVI is defined as:

$$NDVI = \frac{(NIR - red)}{(NIR + red)} \quad \text{Eq. 1}$$

This normalizes all values to a range from -1 to 1. High value indicates temperate and tropical rainforests (NDVI value 0.6 to 0.8), anything less than 0 has no characteristics of healthy vegetation (no green) and anything less than 0.2 means sparse or no vegetation. NDVI is an exemplary method to study vegetation properties, although problems of noise due to fluctuations in atmospheric and soil conditions exists. To avoid this error, X. Zhang et al. (2018), suggested EVI which can limit the rate of background noise. EVI is defined as-

$$EVI = G * \frac{NIR - red}{NIR + C_1 red - C_2 blue + S} \quad \text{Eq. 2}$$

Where C_1 and C_2 are coefficients to correct the red band for atmospheric aerosol scattering, S adjusts the soil factor, and G is a gain factor. The value range of EVI cannot be ensured from -1 to 1 mathematically. Each of these metrics have strengths and weaknesses. X. Zhang et al. (2018) found NDMI (Normalized Difference Moisture Index) to be the most suitable method to investigate mangrove disturbance from a chilling event and severe hurricane. NDMI was proposed by Hardisky et al. (1984) and defined as-

$$NDMI = \frac{NIR - SWIR}{NIR + SWIR} \quad \text{Eq. 3}$$

NDMI values ranges from -1 to +1 and represents biomass and moisture content in vegetation. The relationship among NIR reflectance, vegetation biomass, leaf area index (LAI), and SWIR reflectance is relevant to plant water content are shown as the reason behind the efficacy of NDMI. NDVI is responsive in low biomass conditions but saturate areas with high LAI. Each

vegetation index has its suitability for different environments and specific uses. According to a study conducted by (Xue & Su, 2017), focused on comparative analysis among several vegetation indices, selection of a specific VI should be taken by considering their advantages and limitations. Satellite remote sensing is commonly used to assess forest change (Desclée et al., 2006), often through change detection techniques from two or more satellite images (Johansen et al., 2010). It can be categorized into three groups: (1) visual interpretation, (2) pixel-based methods and (3) object-based approaches (Desclée et al., 2006). Visual interpretation typically uses human expertise to identify changes through analyzing texture, shape, size, and patterns of the images (Lu et al., 2004). Pixel based techniques are based on individual image pixels and allow for quantification between images (Desclée et al., 2006). Analysis of change is possible in two ways using pixel-based techniques. One is detecting simple change vs no-change (e.g. image differencing, image ratioing, vegetation index differencing, principal component analysis), and detailed "from-to" change (e.g. post-classification comparison) (Im et al., 2013). Selecting a suitable change detection technique depends on the study objectives and the environment (Hussain et al., 2013). Nanzad et al. (2019) used NDVI anomalies to monitor drought, whereas Cornforth et al. (2013) used backscatter values of pixels to understand the change in biomass which ultimately identifies a change in forest condition. Pixel based analysis is also used in the Continuous Change Detection and Classification (CCDC) method to develop seasonal vegetation trend model and explore the underlying phenology of forest (Awty-Carroll et al., 2019). Chen et al. (2012) defined object-based change detection as differences in the objects at different periods by using object-based image analysis. Desclée et al. (2006) used OB-Reflectance method to ensure high change detection accuracy by using three SPOT-HRV images. Charrua et al. (2021) used objects-based approach through Land Use and Land Cover classification to explore the

impact of cyclone Idai. Bhowmik and Cabral (2011) classified Landsat images to understand the post-Sidr changes within the species type of Sundarbans and their regeneration pattern. Johansen et al. (2010) concluded that geo-object-based inputs provided more correct change detection than pixel-based techniques.

Much of the research to date has focused on long-term changes in forest cover, land cover, and land use of mangrove forest using an area-based approach (Hoque et al., 2016; Rahman et al., 2013; Islam et al., 2019; Quader et al., 2017; Shapiro et al., 2015; Akhter et al., 2008). For instance, Rahman et al. (2013) used remote sensing tools on different classification methods to detect mangrove forests in the Sundarbans, Hoque et al. (2016) assessed the aftermaths of tropical cyclone Sidr over Sarankhola Upazila within the boundary of Sundarbans, Islam et al. (2019) quantified mangrove cover in Bangladesh by using multidate Landsat imagery, and Akhter et al. (2008) used Advanced Spaceborne Thermal Emission and Reflection Radiometer (ASTER) to analyze Sidr affected areas in the Sundarbans. Only a few studies have focused on the severity of impacts with respect to the condition of mangrove forests and subsequent recovery patterns (see Table 3). Dutta et al. (2015) used MODIS to assess cyclone induced ecological disturbance, Fuller and Wdowinski (2007) mapped cyclone damage and subsequent recovery by using 20m multispectral SPOT and 1km MODIS images of the mangroves of South Florida, Small and Sousa (2019) used Harmonized Landsat Sentinel-2 (HLS) images to map the Sundarbans phenology and disturbance response, Macamo et al. (2016) used pre- and post-cyclone SPOT images to assess changes in mangroves, and Asbridge et al. (2018) used Landsat derived foliage projective cover (FPC), Queensland Global Aerial Imagery, and RapidEye Imagery to indicate that frequent storms can restrict long term mangrove recovery. However, Zhang et al. (2016) took a pixel-based approach where they compared pre and post disturbance

NDMI values of mangrove forest south Florida. In this way, the pixel-based approach can be used to measure the relative condition of mangrove forest at local scales (e.g. pixel or stand level) with respect to disturbance events (Assal et al., 2016). Zhang et al. (2016) found recovery rates of four to seven months for damage from intense chilling events and two to six years from hurricane damage. Studies that focus on recovery from cyclones for the Sundarbans mangrove forest are very few. Several organizations have estimated it might take up to 30 years to recover from cyclone events like Sidr (Reliefweb, 2007), but they give no blueprint for how to measure recovery. Thus, the recovery rate varies based on the location, severity of the disturbance event, and methodology used (see Table 3).

Table 3: Post-Sidr recovery estimation by different studies

Author	**Recovery Period**	**Sensor/Information source**	**Approx. Affected area (sq. km.)**	**High severity area**
(Bhowmik & Cabral, 2011)	3 years	Landsat	2,500	NA
(Awty-Carroll et al., 2019)	11 years (still ongoing)	Landsat	726	NA
(UNESCO, 2007)	10-15 years	Site Visit by the Experts	2,400	NA
(Reliefweb, 2007)	30 years	Experts' opinion	1,400	NA
(Akhter et al., 2008)	NA	ASTER	1,330	148.4
(Dutta et al., 2015)	NA	MODIS	NA	NA

1.7 Objectives and Research Questions

The objective of this study is to assess the impact of cyclone Sidr on Sundarbans (Bangladesh side) and understand the post-disturbance dynamics of this unique ecosystem. I have established two research questions to achieve this objective.

Q1: What was the extent and severity of the cyclone in the Sundarbans with respect to vegetation condition?

Q2: How long did it take the forest to return to its pre-disturbance condition?

Effective selection of a satellite sensor is a key component to answer the above-mentioned questions. Landsat and MODIS are considered in this study. I first determined which sensor met the necessary requirements (e.g., the amount of available imagery in the remote sensing archive, the number of clear sky observations, etc.) to address these objectives.

CHAPTER 2: METHODS

2.1 Study Domain

The Sundarbans mangrove forest consists of 11 Unions (low tier of Bangladesh administrative boundaries), five Upazilas (second lowest tier of regional administration in Bangladesh), and three Districts (highest tier of administrative boundary) (Fig 5). The unions are Khulna Range, Sharankholna Range, Ramjan Nagar, Nalian Range, Chandpai Range and Satkhira Range (Fig 5). This forest also covered Shyamnagar, Koyra, Dacope, Mongla, and Sharankhola which are included in Khulna, Satkhira, and Bagerhat. The main reason for selecting these areas is the trajectory of super cyclone Sidr, which occurred in November 2007. The government Republic of Bangladesh declared Bagerhat as the most affected area and Khulna and Satkhira as badly affected areas after cyclone Sidr (MFDM, 2008).

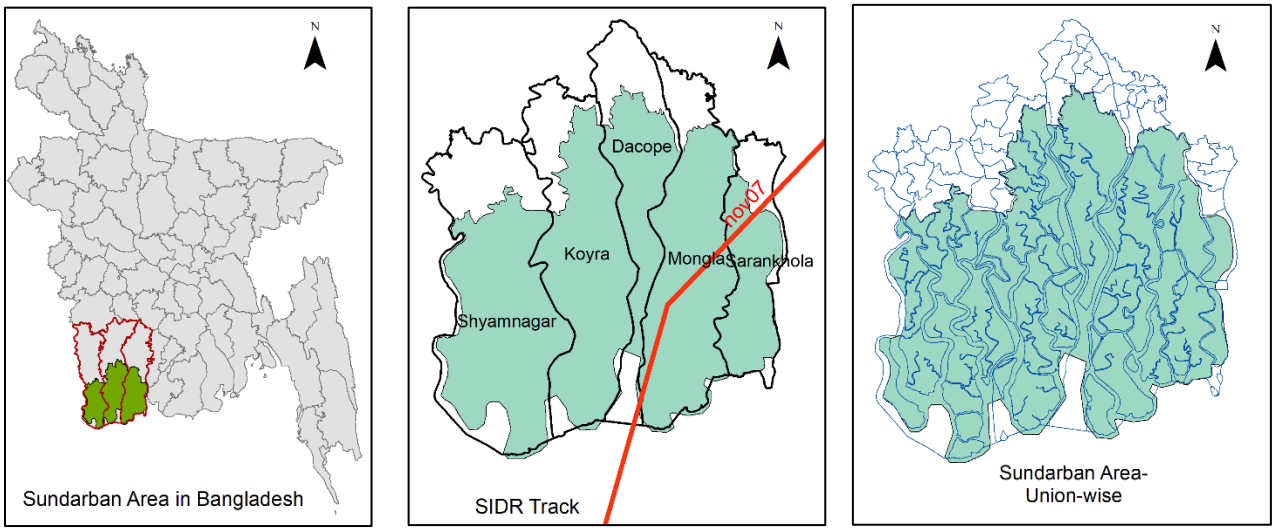

Figure 5: Sundarbans area and trajectory of Sidr over several regions

2.2 Satellite Data

Landsat and MODIS imagery are considered in the study. The goal was to select the optimal sensor to monitor forest disturbance in this area based on considerations such as availability of data in the Google Earth Engine repository, clear sky observations and adequate temporal resolution.

2.2.1 Landsat Data

I started the experiment with Landsat Collection 1 Level-2 (on demand) product (Surface Reflectance Tier 1 in Google Earth Engine). This Landsat product is atmospherically corrected using LEDAPS and provided as surface reflectance. It also included a cloud, shadow, water, and snow mask produced using CFMASK and provides pixel quality attributes as a QA band. Quality assurance bands are used to mask out the clouds, shadows, and water from the images. A Google Earth Engine script was developed to collect Landsat 5 and 7 data for the study. It was necessary to use both sensors, as a single satellite sensor did not provide adequate coverage. Then datasets were merged, and NDMI index was calculated for all images. NDMI proved effective to determine the effects of hurricane events on forests (Wilson & Sader, 2002; W. Wang et al., 2010). Later, the datasets were summarized on a pixel-wise basis. A raster of mean NDMI for each time period was exported as an output of the GEE script. For this study, I considered the window of November, December, and January to explore the available data for the 1990-2011 period. Given the Landsat revisit time for a given path/row is 16 days, we considered the season (three-month period) as our temporal unit. A minimum observation filter was used in the script to ensure the continuous availability of pixels over the study area. A minimum of 2 clear sky observations was defined as the threshold observation filter after considering different levels of thresholds based on data availability. This whole process was

repeated for both Landsat 5 and 7 to ensure data from both sensors. Then the image collections that are found based on the dates and selected filters were merged, and NDMI means were calculated for the periods.

2.2.2 MODIS Data

MOD09Q1.006 Terra Surface Reflectance 8-Day Global 250m product was used in addition to Landsat. This product provides an estimate of the surface spectral reflectance and a QC band to perform quality assurance. Surface reflectance band-1 (620-670mm) and Surface reflectance band-2 (841-876mm) were used to calculate the local monthly mean NDVI. I used the 8-Day composite product instead of daily reflectance because there is an additional QA band. A total of 120 images of mean NDVI for specific months were generated for the 2001-2010 study period. Images were collected monthly basis and through a process of GEE scripting. I established a set of dates for a month to collect images. The state QA Bitmask was used to ensure the quality of pixels. Bit level of 0-1 (cloud state), 2 (cloud shadow), 3-5 (land/water) were considered to create the mask. A minimum number of 4 clear pixels within a month time frame was considered as the threshold. Then the monthly NDVIs and NDVI means were calculated and collected as raster images for further processing in R studio. NDMI requires NIR (near infrared) and SWIR (short-wave infrared) bands to calculate the index while MOD09Q1.006 Terra Surface Reflectance 8-Day Global 250m product doesn't have them both in its profile. So, calculating NDMI using MODIS is not possible, so I considered NDVI from MODIS.

There are numerous tradeoffs between the two sensors. The spatial resolution of MODIS images (250m) is lower than Landsat images (near-30-m) (Fig 6), while MODIS has a higher temporal resolution. Landsat provides coverage on a 16-day repeat cycle, which proved inadequate to monitor forest disturbance due to the scan line corrector (SLC) error in Landsat 7 during the Sidr

period and extensive cloud cover (Chander et al., 2009). MODIS sensor provided necessary data over the study period of 2001-2010 consistently due to its flawless service with shorter repeat cycle. SLC error made it difficult for Landsat to collect consistent data after 2003. Hence, a specific window of 3 months in dry season (November, December and January) was considered so that a parallel comparison can be made between the sensors. Although Landsat data is a primary resource for remote sensing in disturbance studies, MODIS data is becoming prominent in the 21st century (Cohen et al., 2017). Landsat and MODIS efficiency are examined to determine which satellite sensor is appropriate for this study.

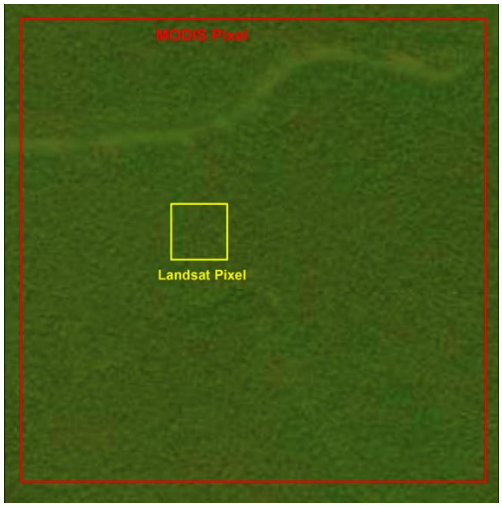

Figure 6: Extent of a MODIS pixel (250X250) and Landsat pixel (30X30) in Sundarbans area. Red box shows the boundary of the MODIS pixel and yellow box shows the boundary of the Landsat pixel (Source: ESRI Base Map).

2.3 Analysis Area

The whole Sundarbans area is divided into two sides, the Bangladesh side and the Indian side. I used only the Bangladesh side of the Sundarbans for this study. A specific Area of Interest (AOI) was prepared based on the MODIS generated images and boundary of the Bangladesh side to perform the final analysis. Google Earth Engine (GEE), ArcGIS, and R Studio were used in different steps to create this specific AOI. A trial polygon was developed in ArcGIS based on the Bangladesh side with an extended ocean area using the WGS 1984 Geographic Coordinate

System and UTM 46N projection system (see Fig 7). Later this trial polygon was converted to a raster using the conversion tools (To Raster>Polygon to Raster) in ArcGIS and snapped to the MODIS generated mean NDVI image to have a MODIS-like final raster with similar spatial properties (Fig 7).

The mean NDVI image from MODIS was reclassified (-Inf to 2180 as No Data and 2180 to Inf as 1; NDVI scale factor = 0.0001) in R to match the value of the converted raster. I determined the threshold using a GIS approach. Mean MODIS NDVI images were overlayed on Google Earth Imagery to check the pixel values in ArcGIS. I checked the values of those pixels which were on the river areas and boundaries and found that most of the pixel values were less than 2180. Therefore, all values below 2180 were determined to represent water and excluded from the analysis. Then this reclassified MODIS image was multiplied by the converted raster to have the master raster of AOI with a value of 1 inside the raster area and No Data outside the area (Figure 7).

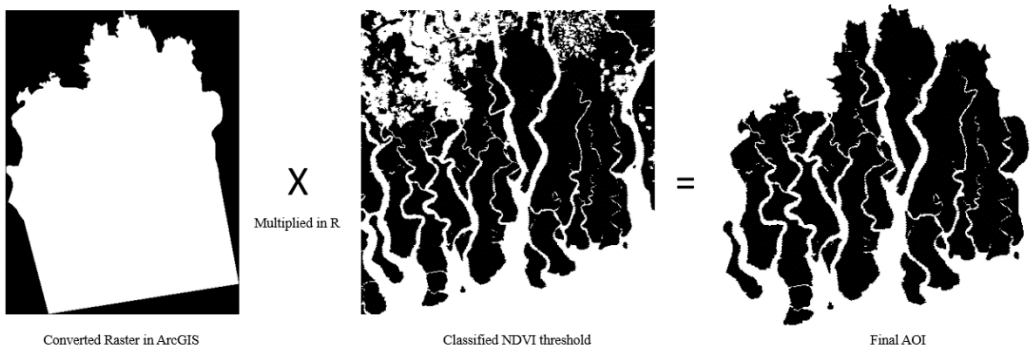

Figure 7: Area of interest processing through developing a master raster

2.4 Analysis

Collecting cloud-free images over the given study period is critical for tropical regions like Bangladesh. The southeast monsoon is the predominant feature of the Sundarbans climate, which

divides the year into three distinct seasons: i) monsoon season—June to October, ii) cool-season—November to February, and iii) spring season—March to June. An important consideration of the study is to collect cloud-less images with respect to clear observations to measure vegetation productivity. MODIS product provided high temporal frequency of clear observations and I considered MODIS over Landsat based on the comparison of Landsat and MODIS (see section 4.1). Monthly mean NDVI composites were generated using Google Earth Engine (GEE), a multi-petabyte open-source catalog of satellite imagery and geospatial datasets by Google (Appendix 1). Clouds, cloud shadows, and water pixels were masked out from the study area before generating the composites. Then composites were developed for the entire study period based on those above-mentioned considerations. A minimum observation threshold of 2-4 clear sky observations was considered, which indicates the minimum number of clear sky observations needed for a given pixel to be considered in the analysis. If a pixel failed to meet is failed to meet the minimum valid observations within a month, then was nullified by the GEE script and considered no data. Composites were generated for every single month within the study period between 2001-2010. Monthly mean NDVI composites were exported from GEE and analyzed in R statistical software (*R Development Core Team*, 2013) to perform the anomalies.

2.5 NDVI Anomaly Calculation

The selection of the optimal window of study (e.g., a month or a series of months with the highest productivity) is important for studying mangrove phenology and dynamics. This window is the ideal annual timeframe when the vegetation of interest is most stable. Data collected during this time is used to compare the performance of the vegetation during a given window against the long-term vegetation conditions of a reference period.

MODIS images from 2001 to 2010 were used to establish the study period. The mean NDVI for an image collection of a month were calculated. A sum of 120 NDVI mean images were generated using GEE, where each image indicates the mean of an individual month collection. Reference periods are selected from this time series. Specific months of 2001-2007 (except November and December of 2007) were selected as reference periods because, at that time, there were no significant disturbances over the Bangladesh side Sundarbans.

NDVI anomalies were calculated for specific months between 2006 and 2010, defined as the deviation from the long-term mean of the reference period. Reference periods were selected on a monthly basis; for example, I selected only the November months before November 2007 (Nov 01, Nov 02, Nov 03, Nov 04, Nov 05, and Nov 06) as the reference period for November 2007. Reference periods for other months were also selected in the same way. The selected months never crossed the year 2007 and the month of November; for example, the reference period for December 2008 is selected till December 2006 (Dec 01, Dec 02, Dec 03, Dec 04, Dec 05, Dec 06). This specific selection is essential to maintain uniformity among the reference periods considering Sidr made landfall in early November 2007. Anomalies were calculated until 2010 as Bangladesh witnessed another cyclone in 2011, which may mislead the Sidr specific analysis if taken into consideration. An anomaly is calculated for the selected month of a year (January 2006-December 2010) by taking the difference between the chosen month mean and reference period mean, then dividing by the standard deviation of the reference period (Toomey et al., 2011) (Eq 4). The equation can be constructed as below-

$$NDVI\ anomaly = \frac{NDVI_{mean\ of\ a\ specific\ month} - NDVI_{mean\ of\ reference\ period}}{NDVI_{standard\ deviation\ of\ reference\ period}} \quad \text{Eq. 4}$$

Since the anomaly values are normalized by the reference period standard deviation, they are referred to as z-scores (Toomey et al., 2011). Upon classifying the z-scores at a later step, these values ultimately represent the severity of the event.

2.6 Reclassification and Summary Analysis

To facilitate area calculations, anomaly composites were summarized and reclassified into groups. I established six seasonal composites (Dry Season 2007, 2008, 2009 and Wet season 2008, 2009, 2010) for this study. Dry seasons were combined of November, December, and January while the wet seasons were combined of June, July, August. The mean of the seasonal composites was calculated and classified into four zones, High (z-scores < -5), Moderate (z-score >-5 and <-2.5), Low (z-score >-2.5 and <-1), and Neutral (z-score >-1 and <+1) (see Table 4). Areas greater than 1 are enriched with vegetations or not damaged as per analysis. This classification indicates the severity of the damage, e.g., the lower the z-score the severe the damage. Colors are assigned based on the severity in the maps (Table 4).

The monthly MODIS anomaly z-scores were labelled into anomalies as mentioned above and categorized into different dry seasons based on the months. Dry seasons are the best window to get clear sky observations than wet season in countries like Bangladesh. Moreover, image availability is also high during the dry season. I couldn't get sufficient Landsat observations per month during the study period except the months of November, December, and January which are considered Dry season as a whole for this study. Hence, considering wet season (June, July, and August) as a part of this study was difficult. The wet season months showed a good amount of No Data after imposing minimum observation threshold. Later this study continued based on the Dry Season and MODIS sensor to avoid the problem of No Data. It's difficult from Landsat

sensor due to its 16 days revisit time. That's why this study focused on dry season than wet season.

Table 4: Severity zone classification based on z-scores

Severity Zones	**Z-Scores**
High	< -5
Moderate	>-5 to <-2.5
Low	>-2.5 to <-1
Neutral	>-1 to <+1
Normal	>1 to <2.5
Normal	>2.5 to <5
Normal	>5 to Inf

CHAPTER 3: RESULTS

3.1 Sensor Selection

Landsat and Moderate Resolution Imaging Spectroradiometer (MODIS) were both considered in this study. The availability of clear sky observations was a key consideration in sensor selection to address the objectives of this study. I was unable to obtain enough clear sky observations for a given window using Landsat data. This was not entirely unexpected as Landsat has a longer revisit time (e.g., 16 days per path/row image) compared with the MODIS product used (e.g., 8-day composite). Landsat 5/7 provided an average of 1.24 clear sky observations per pixel per month over the study period (2001-2010), while MODIS provided 3.81 clear sky observations per pixel per month (Fig 8, panel b and c). In the dry season (November, December, and January), MODIS provided 3.93 observations per month while Landsat provided 1.67 per month. During the wet season (June, July, and August), these numbers dropped to 1.05 observations per pixel per month for Landsat (Fig 8). It is important to note the clear sky observations were not consistent across the study area, so some locations had substantial temporal gaps in data. Therefore, we used MODIS imagery for continued analysis.

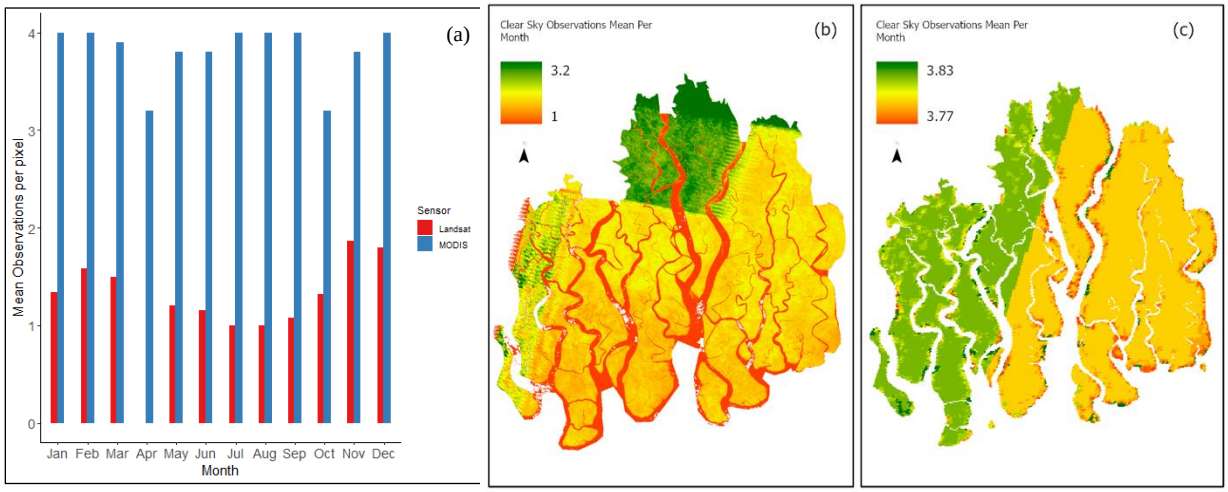

Figure 8: (a) The comparison between Landsat and MODIS clear sky observation means over the months is shown with red color (Landsat) and blue color (MODIS). Mean clear sky observation maps for the study area (b) Landsat and (c) MODIS.

3.2 Extent and Severity

Anomalies were calculated based on the mean and standard deviation of the reference period for specific months. The extent of the storm's impact was calculated by tabulating the area of classified severity zones based on the z-scores. The dry season anomaly of 2007 highlights the extent of the damage that occurred right after the cyclone (Fig 9, panel A). Red and orange pixels show the high and moderately affected area which is high on the trajectory of Sidr and its surrounding areas. South-eastern areas are most affected areas while the north-most areas are less affected and south-western areas are moderately affected based on the severity scale and extent of affected areas. This is consistent with the approximate path of the Sidr (Figure 5). As the south-western and north-most areas are moderately and less affected, they recovered quicker than the south-eastern areas (Fig 9, panel G). It is likely the November 2007 anomaly showed less damage than December 2007 and January 2008 anomaly because November 2007 contains some pre storm pixels. Pre storm pixels exist because Sidr hit Sundarbans in the middle of November. The deviation in severity is clearer in the December 2007 and January 2008 anomalies compared to the November 2007 anomaly.

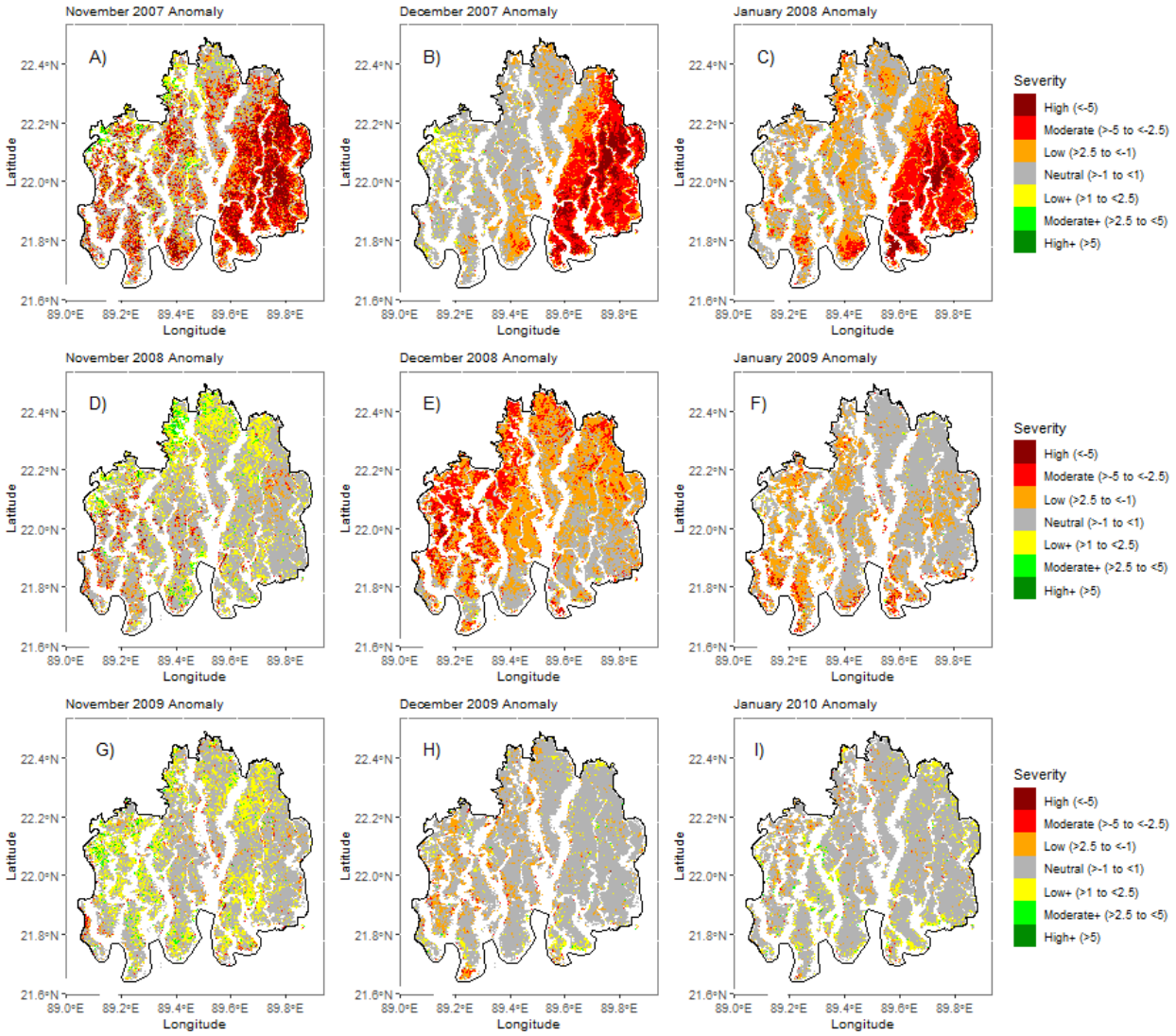

Figure 9: Monthly dry season anomalies (November, December, and January) in 2007, 2008, and 2009. Negative anomalies represent damage compared to the reference period; whereas positive anomalies represent areas that performed higher than the reference period.

The dry season 2009 showed less variability in the high severity zone than the dry seasons of 2007 and 2008, indicating recovery of the areas heavily affected by Sidr (Fig 10). During this same time, neutral zones increased in area from dry season 2007 to 2009. The median of the z-scores in neutral pixels was -0.32 in dry season 2007. However, it increased to 0.17 in dry season 2009, although the high severity pixels were always increasing at a slow rate. The median values of high severity pixels for dry season 2007 is -5.83 while the value remain slightly unchanged (-

5.98) in dry season 2009 too. On the other hand, moderately and low affected pixels showed improvement in median values over the dry seasons which added more relevance to the recovery question. The median of the moderately affected pixels decreased from -3.62 in dry season 2007 to -2.86 in dry season 2009 (Fig 10). Besides, the median of the low affected pixels also decreased from -1.6 to -1.28 in dry season 2009. These changes collectively indicate continuous post-Sidr recovery during that time period.

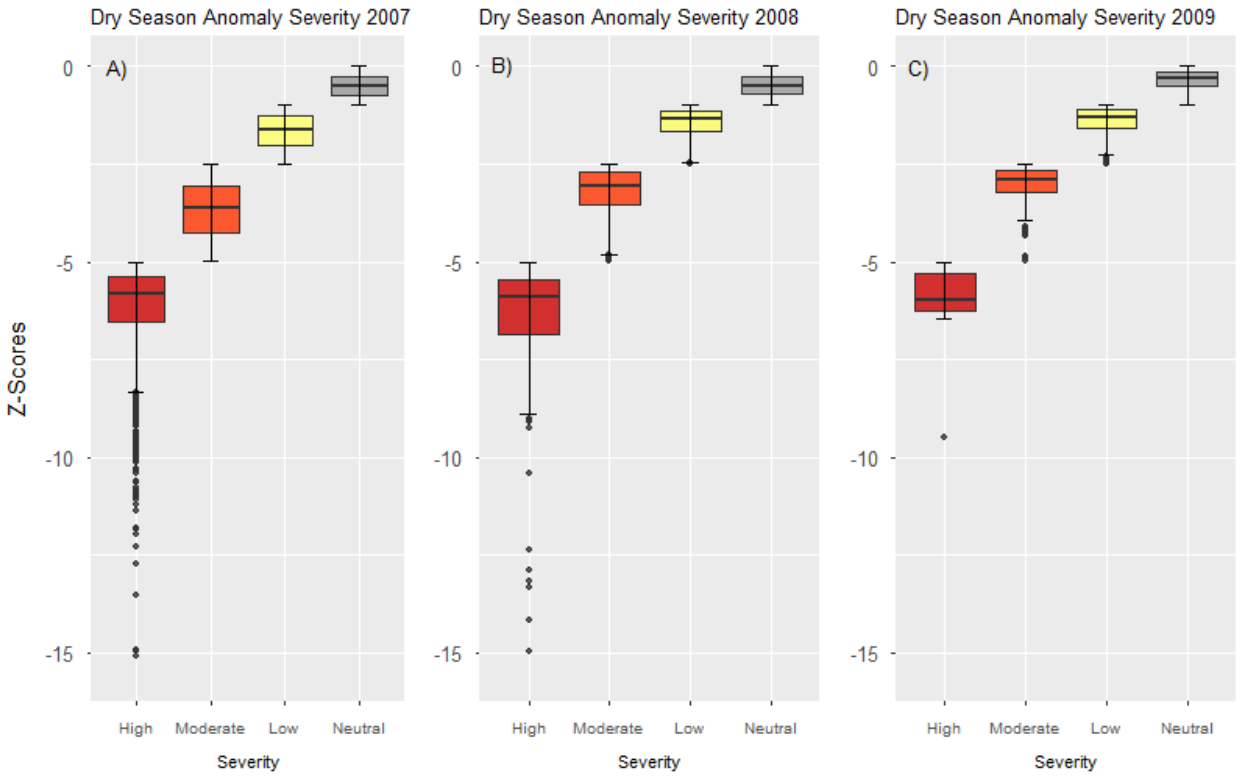

Figure 10: Dry season anomalies based on severity zones, (A) Dry Season Anomaly Severity 2007, (B) Dry Season Anomaly Severity 2008, and (C) Dry Season Anomaly Severity 2009

A total 2261 sq. km (approx.) area was impacted by cyclone Sidr during dry season 07, which is approximately 37% of the total Bangladesh Sundarbans area (total area 6000 sq. km). The amount of damaged area was reduced to approximately 1782 sq. km in dry season 08 and just 136 sq. km in dry season 09 (Fig 11). This study found a decline in the area of Sundarbans impacted by Sidr from dry season 07 to two other dry seasons (08 and 09) by 21% and 93%

consecutively. This decline indicates that damaged areas were slowly recovering from the cyclone's impact. An increase in the number of neutral areas (z-score >-1 to <+1) was also observed during the three consecutive dry seasons. There were 1355 sq. km with a neutral score during dry season 2007. This increased to 1783 sq. km in dry season 2008 and 3040 sq. km in dry season 2009 (Fig 11, panel C).

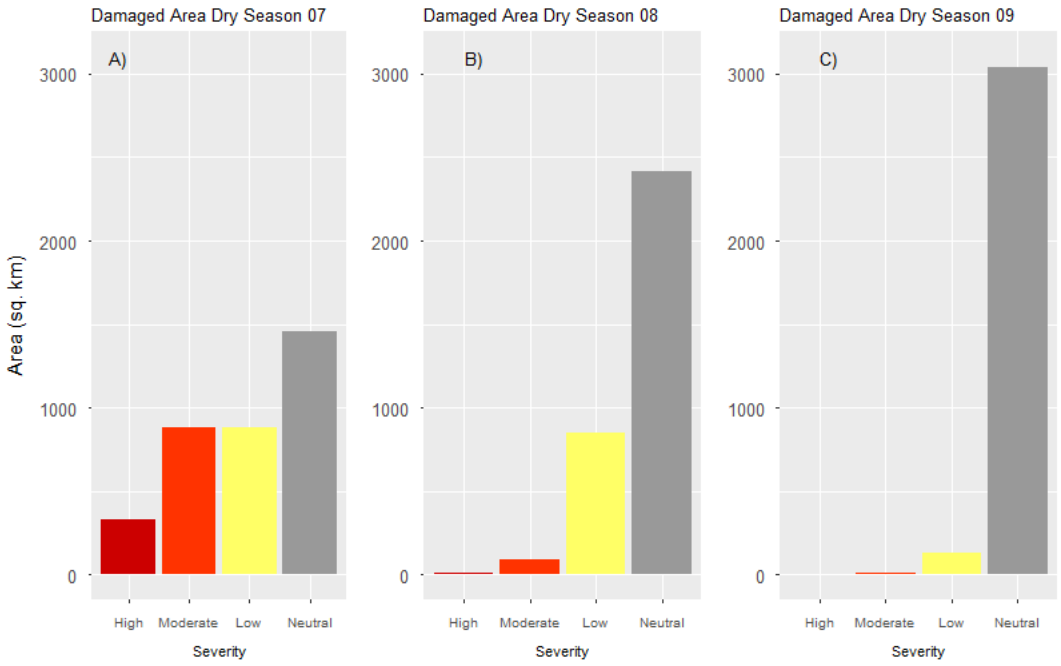

Figure 11: The extent of post-Sidr damaged areas based on, (a) dry season 2007, (b) dry season 2008, and (c) dry season 2009. Units are in square kilometers.

3.3 Post-Sidr Recovery

The recovery of z-scores, leading to a decrease in the size of high severity areas, coupled with an increase in area of with neutral z-scores, are all considered as recovery measures from Sidr. The number of high severity pixels decreased by 88% and 98% from dry season 2007 to dry season 2008 and 2009 consecutively (Fig 12). The number of high severity pixels was 18,086 in dry season 2007, 2027 in dry season 2008, and 304 in dry season 2009. A decline in the high severity pixels was also observed between the months in each season. For dry season 2007, the pixels

were reduced by 55% from November 2007 to December 2007, 28% from December 2007 to January 2008, and 67% from November 2007 to January 2008. For dry season 2008, the pixels were reduced by 58% from November 2008 to January 2009, 67% from December 2008 to January 2008, but a rise by 22% was seen from November 2008 to December 2008. For dry season 2009, the pixels were reduced by 70% from November 2009 to December 2009, 89% from November 2009 to January 2010, and 64% from December 2009 to January 2010 (Fig 12).

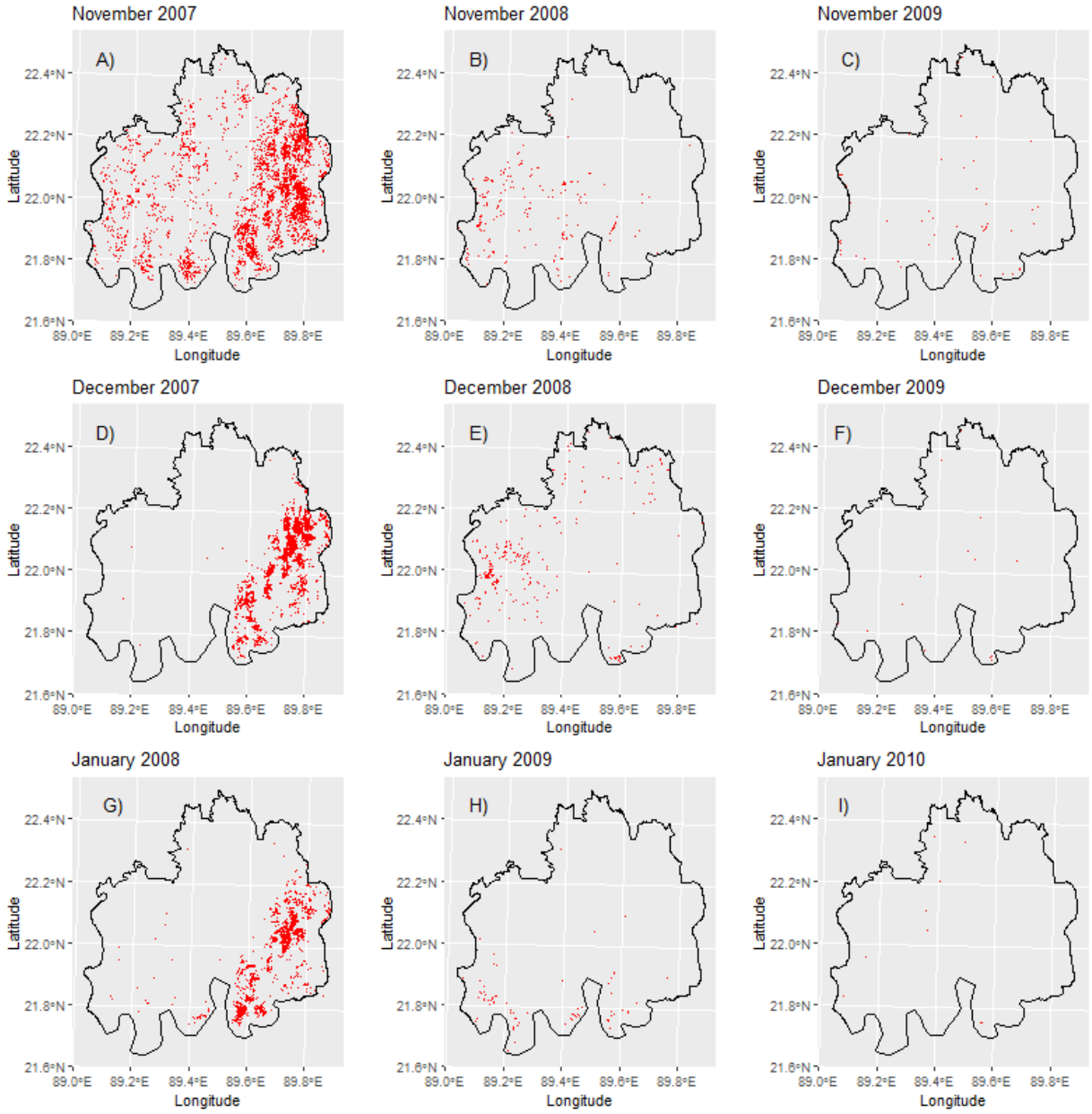

Figure 12: Red pixels are shown to present the high severity pixels and their progression over the months and seasons.

CHAPTER 4: DISCUSSION

4.1 Extent and Severity Cyclone Sidr

I used MODIS to explore the severity and extent of cyclone Sidr, which enabled me to perform a broad spatiotemporal assessment. Given the MODIS pixels (250 x 250 m) are larger than Landsat pixels (30 x 30 m), there is a greater possibility of non-uniform landscape change in any given MODIS pixel (Fig 6). However, the greater temporal frequency of MODIS provides an opportunity to assess post-disturbance damage more consistently and quickly. It's possible to understand the changes in MODIS very soon after the disaster event; however, given the differences in spatial resolution, at least 70 Landsat pixels are required to match one MODIS pixel. Quick assessment demands a high temporal resolution from daily to monthly scales and a high percentage of clear sky observations. This is a critical factor in the Sundarbans due to high cloud cover associated with tropical climate conditions. I obtained 120 monthly mean NDVI images with a minimum of four clear sky observations using MODIS, while I had to use a threshold of two for Landsat images during a three-month seasonal period to ensure there were not a large amount of No Data pixels in my analysis area. There were many missing pixels values in Landsat data between November (2007) and February (2008). This is a critical time period to understand the immediate impact of Sidr on the landscape. Continuous data is critical to understand how the post-disturbance changes evolve over time; therefore, I used the MODIS satellite sensor to ensure the data availability necessary for a rapid assessment. This enabled the development of temporal severity zones based on the z-scores for the dry season at a monthly time step. There was extensive flooding of vegetation and coastal areas in the aftermath of Sidr. Given that water has very low NDVI values, the MODIS NDVI composites likely tracked

inundation. These depressed NDVI values, which represent part of the disturbance impacts, would have been missed by an approach that did not use multiple observations in each time-step.

This method used a reproducible approach as I used Google Earth Engine scripting where any researcher can download sensor-specific images anytime. Due to this approach, anyone can replicate it for their research and study area. I used the same script for both Landsat and MODIS products with a slight modification of the sensor information, band information, and cloud mask process as they are different from each other. This method is not computationally expensive and most of the sensor images are available in the Google Earth Engine cloud platform and easily accessible. Shareable scripts can be edited by any researcher who has access to it. Most of the detection change analysis and map trends are possible to accomplish in Google Earth Engine using massive cloud storage. There is no simulation model used in this study to ensure the uniqueness of this research and make it more relevant to real-life scenarios.

I used a known reference period to compare the study periods in different seasons. This study compared specific months after Sidr to those specific months before Sidr as a reference period to maintain uniformity in analysis; for example, post-Sidr Novembers are compared with pre-Sidr Novembers. Known reference periods provide a baseline to understand NDVI variability during a given time-period (e.g., one month), with assumed consistent inter-annual phenology. Typically, weather patterns for specific months are similar, and considering them as a reference period ensures uniform comparison. In that way, the known reference period is useful for having some pre-analysis information and concept about the months and study area. Using all of the months as one reference period can be misleading to explore because not all the months of the year share consistent weather conditions and/or vegetation phenology patterns. It's also possible that valid data is not available for certain months in a year, creating data gaps and adding

uncertainty to the results. Considering all the months over the study period may show more vague variability than known reference months. I avoided the months affected by other cyclones than Sidr in my research which was not possible if I included all the months in the reference period.

The most impacted landscape feature during a robust tropical cyclone is vegetation. Disturbances are a natural component of this ecosystem (Hobbs & Huenneke, 1992), but the high wind power of a tropical cyclone can cause extensive damage to vegetation. Sidr damaged 2,261 sq. km. of the total area of Sundarbans (Bangladesh Side) during November 2007- January 2008; approximately 37% of vegetated areas (dense and sparse). My study identified severe vegetation damage through the path of the cyclone (south-eastern side), moderate and less severe damage in areas (south-western and north-western) that are at a distance from the storm's trajectory, which is expected after a cyclone of 4-category (Krauss & Osland, 2020). Vegetation outside of Sidr's direct path were likely damaged from the high winds associated with the storm event. Several other studies reported damage from Sidr in similar areas (Bhowmik & Cabral, 2011; Awty-Carroll et al., 2019; Akhter et al., 2008). My findings are consistent with several others that found the eastern and south-eastern parts of the Sundarbans were most severely affected, while the northern part was the less affected area (Akhter et al., 2008; Bhowmik & Cabral, 2011). Akhter et al. (2008) showed that 1,330 sq. km. of Sundarbans was damaged by Sidr, using Advanced Spaceborne Thermal Emission and Reflection Radiometer (ASTER) images of 21 November 2007. However, this study only used imagery from a single day and only covered a portion of the Sundarbans. As such, they were unable to capture delayed tree mortality from Sidr. Therefore, it is not directly comparable to my study which captured the long-term impact of delayed tree mortality across the entire Bangladesh side Sundarbans. Bhowmik and Cabral

(2011) reported approximately 2500 sq. km. was damaged due to Sidr, using annual Landsat classifications of cover types. This is consistent with my findings and highlights the compatibility of different approaches and sensors. Although MODIS has reduced spatial resolution, it is consistent with Landsat based results. However, it offers the additional temporal resolution for rapid assessment using monthly anomalies. Awty-Carrol et al. (2019) estimated damage around 726 sq. km. (considered total area of the Sundarbans as 6,600 sq. km.) using Landsat data from 1998 to 2018. However, they note their approach, using the Continuous Change Detection and Classification (CCDC) method was impacted by the SLC error from Landsat 7 (September 2007 to February 2008), which contributed to their lower damage estimate. They also report 345 sq. km. of those damaged areas were not recovered by mid-2018 and showed that most of the recovery of Sundarbans occurred between 2013 and 2018, which is inconsistent with our results and Bhowmik and Cabral (2011). Bangladesh experienced several other cyclones in that period which might skew the results as well. During their study period (1988-2018), Bangladesh was hit by 17 cyclones (BMD, 2017). Finally, Dutta et al. (2015) used MODIS Enhanced Vegetation Index (EVI) and Land Surface Temperature (LST) products and found a 50% decrease from pre-Sidr EVI in the extreme eastern portion of Sundarbans. Although my study used NDVI, the results show agreement across multiple approaches.

The aforementioned studies did not consider a change based on a season, rather they focused on months or days. I focused on season-based analysis, e.g., the primary months from dry to dry season, to depict the changes. Due to the tropical climate, it's not possible to obtain consistent clear sky images over the Sundarbans area, which may mislead the results if taken into consideration. My results are mostly consistent with studies that used single date imagery at key points in time; however, the use of MODIS imagery in this study enabled season-based analysis

with a robust reference period-based comparison and provides another line of evidence on the impact of Sidr.

The calculation of anomalies is a quick analysis that compares any study period (e.g., a month) with a known reference period. In a climatic variability context, a cyclone is a temporary condition, so anomalies are one of the most effective ways to explore the deviations from a normal period (Nanzad et al., 2019). Previously it was prominently used as a drought monitoring index as per Nanzad et al. (2019), but I am using it for the cyclone impact monitoring index. A series of NDVI values shows the trend in vegetation, while an NDVI anomaly shows the deviation of NDVI from a certain period to get a clear view of the deviation in conditions. Furthermore, anomalies are calculated using a basic equation in an open-source environment. Collectively, this is highly reproducible approach that offers rapid post storm assessment.

4.2 Cloudy Pixels Increase Uncertainty

Continuous observations are essential for change detection study, yet this poses a challenge in tropical areas. The climate of Bangladesh is not favorable to produce continuous clear sky observations throughout the year. Bangladesh records a lot of rainfall during June-September, and it is typically considered the rainy season. The winter season runs from mid-October to February. This is the best window to obtain clear sky images because of low probability of cloud cover, compared to the rainy season (Fig 3). Hence choosing a sensor based on the amount of available cloud free imagery was critical to this study. This study started image collection and analysis with both Landsat and MODIS, two prominent sensors to conduct long-term time series analysis.

Cloud cover, and the subsequent number of minimum observations, was the most crucial consideration for choosing the sensor used in the study. Quality Assurance bands were used to masked out the cloud, cloud cover, and water using Google Earth Engine. However, Landsat did not provide continuous clear sky observations after masking out the clouds. This sensor provided at least 1 clear sky observations for 60 months of the study period (120 months from 2001 to 2010) and none for rest of the months. Since this is not a single image-based study, cloudy pixels were a threat to long-term image collection. I enforced a minimum threshold of 2 clear sky observations, but still, for many months, Landsat provided just above one observation for much of the study area. MODIS provided 120 images in that time period with a mean observation of more than 3 per month across the study area. Quality assurance bands were used to mask out the cloud, cloud shadows, and water pixels. Later clear sky observations were selected based on the minimum clear sky observations approach. MODIS provided more clear sky images than Landsat within the study period, so MODIS was chosen over Landsat for this study. The high temporal frequency of MODIS (8-day) was always a major reason to choose it over Landsat (16-day) too.

Using NDVI anomalies is one of the simplest methods to detect change between seasons and to compare seasons to a known reference period. Since I categorized the seasons in the dry season and wet season, I used anomalies to compare them (Eq 4). Some other forest monitoring methods in the research domain are also prominent, such as the Breaks for Additive Seasonal and Trend (BFAST) (DeVries et al., 2015), Landsat-based Detection of Trends in Disturbance and Recovery (LandTrendR) (Kennedy et al., 2010), and the Continuous Change Detection Method employed by Awty-Carroll et al. (2019). R-based implementation of BFAST is time-consuming as it may take at least one week to perform analysis on a Landsat time series longer than five

years with a standard computer setup (16 GB of RAM and 8 CPU cores) (Hamunyela et al., 2020).

However, thresholds to identify the magnitude of change in forest areas can be misleading using this approach. In that way, disturbances with magnitude values lower than the defined threshold have a chance of being overlooked. DeVries and colleagues (2015) reported they couldn't perform regrowth and repeat disturbance detection using BFAST in their research on tropical montane forest disturbance monitoring for several reasons, including persistent cloud cover (DeVries et al., 2015). LandTrendR focuses on the spectral trajectory of a pixel and detects changes from its stability and breakpoints. An abnormal downward trend in spectral history provides a signal of negative change, possibly due to a disturbance. LandTrendR can provide information about the duration and recovery time of a pixel, while an anomaly calculation normalizes deviation with respect to each time period, allowing for direct comparison between seasons. As such, the LandTrendR algorithm is highly dependent on the availability of continuous observations throughout a year (Kennedy et al., 2010). However, my study focused on season-based comparison because of the difficulty of getting enough clear pixels all year. In addition, I was unable to obtain enough clear sky observations with Landsat (Fig 8), which was the sensor of choice when LandTrendR was designed. MODIS can continuously provide images in a higher temporal scale which is very effective to conduct anomaly calculations for specific periods.

A consideration of minimum observations is essential in a change detection study involving a dynamic environment such as the mangrove forests of the Sundarbans, yet it is often overlooked (Charrua et al., 2021; Dutta et al., 2015; Awty-Carroll et al., 2019; Zhang et al., 2016). For example, a single image is only a single snapshot of the landscape, and as such could lead to

spurious conclusions about the amount of change an area has experienced (Assal et al., 2021). A more robust approach is to consider a minimum number of observations over an observation window and calculate the mean during that time. It is not always possible to get clear sky images during a given time period in a specific study area. In that case, a minimum number of pixels should be valid within a time frame to be considered as quality pixels in a study. If a study month doesn't meet the minimum number of observations, there could be a higher amount of uncertainty in the mean NDVI value if a single observation occurred at the beginning or end of an observation window. Considering observations have a critical role in different trend analysis studies, for instance, (Charrua et al., 2021) considered data from three Landsat (7 ETM+ and 8 OLI) scenes per April month for consecutive eight years (2012-2019). The authors considered April only because cyclone Idai hit Mozambique in March 2019. So, the change study is based on April observations, while a cyclone may have lag effects on the vegetation in subsequent months. However, they didn't enforce a minimum observation threshold in their study, and as such, some pixels values could reflect a single date Landsat observation. Therefore, my study considered a seasonal-based approach with a minimum observation threshold enforced to reduce the uncertainty of observations following effects of cyclone Sidr. Furthermore, they did not provide background on the reference period (2012-2019), however, there could have been a cyclone in 2011 or before that. As per the study, the last cyclone before 2019 was in 2003 (cyclone Japhet). The omission of observations from 2004-2011 is not understandable. A minimum observation consideration should be placed in the script or algorithm to conduct analysis based on valid observations. My study considered 2 (two) minimum observations per month for Landsat and 4 (four) for MODIS. I considered those pixels in my study area which fulfilled these threshold criteria to be considered for analysis. Minimum observations are

important to ensure uniformity and reduce uncertainty in the study period because not all months can provide the same number of valid observations, particularly in tropical areas like Bangladesh. I obtained 58 months within 120 months of my study period having at least one clear sky observation from Landsat, while I found 120 months out of 120 months with at least three clear sky observations from MODIS. The importance of clear sky observations is noted in other studies (DeVries et al., 2015; Assal et al., 2021), whereas my study also used quality assurance flags to remove unacceptable pixels before calculating clear sky observations per month per pixel.

4.3 Post-Sidr Recovery and Long-term Vegetation Dynamics

According to the results of my study, Sidr damaged approximately 2,261 sq. km. (37% of the total area) in the Bangladesh side of the Sundarbans. Over 2100 sq. km recovered by the dry season 2009 (November 2009, December 2009, and January 2010), a decline of 93%. The recovery is visible from November 2007 to January 2010 (Figs. 9 and 12). Although a continuous monthly timeline is not confirmed, Sundarbans vegetation recovered substantially within three years from the event. Bhowmik and Cabral (2011), using a Landsat and species-based approach, found that Sundarbans recovered completely by 2010. The authors concluded that the rate of regeneration is related to species type. Conversely, Awty-Carrol et al. (2019) reported approximately 345 sq. km. of damaged pixels had not yet reached pre-Sidr level NDVI values by 2018. They noted a more rapid increase among the pixels between 2013 and 2018 than between 2007 and 2013 using their CCDC model. The authors mentioned quick recovery of less exposed pixels and positive biasness of Landsat 8 NDVI, beginning in 2013, as reasons for this recovery difference. Environmental changes and several other cyclones over the study area were noted as possible reasons behind the rate. Reliefweb (2007), a prominent global crises and

disaster information portal, reported an approximate 30 years for recovery based on the statements of the national experts. However, this rate of recovery is much longer than estimates as reported in the literature and is only an assumption without any scientific research. The UNESCO (2007) also predicted a recovery of 10-15 years based on their expert's opinion after conducting a field visit to the affected areas. This prediction is also based on opinion rather than a data driven analysis.

Different recovery estimates are possible as studies use different methods, spatial areas, time periods and imagery. I found an approximate three-year recovery period, which is similar to one study and differs from others (Table 3). High severity pixels were reduced from Sidr period to 2010 which is an indication of recovery. Cyclones are very frequent disaster events in Bangladesh which can compound the recovery period of a single disaster event. This country witnessed cyclone Rashmi and Aila right after Sidr within a time span of 3 years (Table 2).

Given these issues and the range in the reported results of Sidr extent and severity, I conducted a study using a different approach. Although there are strengths and weaknesses of all the studies, the ability of my approach to quickly detect change associated with cyclonic storm events could hold great value for rapid post-damage assessment. However, the coarse spatial resolution of MODIS data, and the associated spectral mixing, makes it more difficult to determine the precise rate of vegetation recovery. Therefore, my study contributes additional information about this storm event, and in turn, provides another line of evidence about this historic ecosystem disturbance (Assal et al., 2014).

4.4 Damaged caused by other cyclones after Sidr

Dutta and colleagues (2015) conducted a comparative analysis on ecological disturbance in the Sundarbans caused by cyclone Sidr, cyclone Rashmi, and cyclone Aila using MODIS time-series data from 2001 to 2011. They reported damage from Sidr occurred from the west to the east side of the Sundarbans, consistent with my results. However, the Sundarbans were hit by another cyclone called Rashmi on October 25, 2008, less than one year of Sidr. This cyclone made landfall at the southern part of Bangladesh's side of the Sundarbans at a velocity of 93 km per hour (Table 2). They report a decrease in EVI values, but substantially less so than with Sidr's impact. However, they note there was likely compound damage from Sidr and Rashmi. Less than one year after Rashmi, Cyclone Aila made landfall on May 23, 2009, with a wind speed of 111 km per hour (Table 2). However, cyclone Aila hit the Indian side of Sundarbans directly (950 km south of Kolkata) but had a significant impact on the ecosystem due to 6.1m high tidal surges (Dutta et al., 2015).

Whereas Sidr and Rashmi had clustered impacts, the impact from Aila was distributed all over the Sundarbans and not in a uniform pattern. Aila added a new dimension to the ongoing recovery of Sidr and Rashmi. Since Aila made landfall in summer, during the height of the rainy season, its immediate impact was not captured by my analysis until the following dry season (Nov. 2009). My study illustrated the extent of cyclone Sidr until 2010, and the recovery from 2007 to 2010. However, this recovery was likely interrupted by cyclones Rashmi and Aila. Although the method used by Dutta and colleagues couldn't capture the impact of post-Sidr 2007, as it hit the forest during the peak growing period (December-January). but highlighted subsequent impact from Rashmi and Aila can explain the recovery delay of Sundarbans. These findings highlight the challenges of addressing cyclonic impacts in an area prone to these events.

It is very difficult to address the vegetation recovery question if the impacts of multiple storm events cannot be decoupled. This could explain in part why Awty-Carrol et al. (2019) reported the Sundarbans vegetation had not yet recovered from Sidr (as of 2018).

Although these considerations highlight potential pitfalls of time series research, it clarifies several things about my study. The approach I used is very straightforward for quickly determining the extent of a cyclone's impact that occurs at or just before the beginning of the dry season. Assessment of cyclones that occur during the rainy season are impacted by fewer clear sky observations, thus increasing the uncertainty of those findings. Finally, the collective literature and my findings confirm that recovery assessments are a future research need at this time.

4.5 Limitations and Future Needs

Field verification data are always important for this kind of research. However, due to the pandemic, I was unable to conduct a field visit to Sundarbans, which could shed some additional light on my results. I collected and verified data from secondary sources, e.g., literature, websites, etc. Images were collected from sensors, and results were compared and verified with other Sundarbans, mangrove ecosystems, Sidr impact-related literature. The phenology cycle of the forest, ecosystem, climate pattern, geographic location and vulnerability, floral diversity, fauna diversity, related livelihoods, growing season are all important in a mangrove study. Knowing the study area well always provides an advantage to explore the recovery pattern from disturbance events and develop questions and assumptions for research. For instance, mangroves recover quicker than other ecosystems, which can be helpful to compare with the calculated recovery from image analysis (Awty-Carroll et al., 2019). Deeper questions related to the forest adaptation to regular disturbance events can be answered by understanding the study area

thoroughly. There can also be other reasons for decreasing vegetation levels, which has a huge possibility to be interpreted as natural disturbance from image analysis. Such issues can be minimized through field validation.

The spatial resolution of MODIS (250m) compared with Landsat (30 m) also represents a limitation. Data misinterpretation can be possible from the MODIS sensor due to this coarse spatial characteristic. In a pixel of 250m, many ecological processes can be occurring at the same time. A low NDVI value might not represent decreasing greenness of all the trees in a pixel; maybe only a portion is in decline. In the same way, a high NDVI value doesn't necessarily indicate the vegetation health is good across a given pixel. Some parts of it can be damaged but didn't reflect in the main pixel analysis due to the coarse nature of the MODIS pixel. However, the temporal resolution of MODIS is very effective for change detection analysis, particularly for areas like Sundarbans, where the climate is a huge obstacle. Conversely, Landsat has a finer pixel of 30m where changes can be easily detected at a more precise spatial scale, but the temporal resolution is not favorable for my study area. Therefore, both the sensors have limitations based on the study area.

Sensor selection is always an important consideration factor in this kind of research. More extensive research is required to select the best possible sensor according to the study area. Tropical areas are critical to have enough clear sky observations due to climatic patterns, limiting multi-spectral sensors like MODIS and Landsat. Future studies on this area could be done using Sentinel-1 Synthetic Aperture Radar (SAR) data. Sentinel-1 provides continuous all-weather data with day-and-night imagery. Besides that, Sentinel 2A/2B combined with Landsat Data Continuity Mission (LDCM) will provide a 5 days of revisit time and 8 possible high resolution

observations per month which might add a new prospect in forest monitoring for future disturbances (Zhu et al., 2012).

Climate change and anthropogenic factors are ignored in this study due to my focus on a single cyclonic event. Climate change influences tropical cyclone frequency and intensity (Krauss & Osland, 2020). The potential impacts on mangrove forests are expected to increase in the future, therefore the relationship between climate change and mangrove forest recovery is a research need (Krauss & Osland, 2020). This information would be a valuable contribution in better understanding the role of recovering mangrove forests in storm surge scenarios associated with future cyclone events (Deb & Ferreira, 2017).

My analysis illustrates the use of MODIS anomalies as an effective method for rapid post-disturbance assessment. However, many disturbances are occurring in the forest besides natural disturbances like a cyclone. Therefore, any assessment must be coupled with additional approaches to determine the recovery of cyclonic disturbances. Recovery patterns and probable delay response from ongoing disaster events is a research need, confirmed by the conflicting results of the literature reported her

CHAPTER 5: CONCLUSION

This study aimed to explore the extent and severity of cyclone Sidr, which made landfall in November 2007 over the mangrove forest of Bangladesh, Sundarbans. It took several reference periods to calculate the extent and severity from 2006-2010 using NDVI anomalies. Imagery from the MODIS sensor was used in Google Earth Engine to generate mean NDVI data. An attempt was also considered to calculate the probable recovery of Sundarbans vegetation from Sidr. The results showed that the eastern side of the Sundarbans were severely damaged compared to the west and north side. Sidr made landfall on the east side of the Sundarbans, so higher levels of damage on the east side was expected. Approximately 2300 sq. km. were impacted by Sidr, approximately 37% of the total area. The vegetation of the Sundarbans showed a gradual recovery from 2007 to 2010. The area was hit by cyclone Rashmi and Aila during the study period. Therefore, my results include the impacts from these cyclones in the anomaly maps. The anomaly methods used in this study are novel for the Sundarbans and provide another line of research to determine rapid post-cyclone assessments. These products can be helpful for disaster management and forest management authorities to take action to manage forest recovery efforts. Future research related to forest recovery from frequent disaster events, under a changing climate, can build on their results of this study.

REFERENCES

Ahmed, B., Kelman, I., Fehr, H. K., & Saha, M. (2016). Community resilience to cyclone disasters in coastal bangladesh. *Sustainability (Switzerland)*, *8*(8), 1–29. https://doi.org/10.3390/su8080805

Akber, M. A., Patwary, M. M., Islam, M. A., & Rahman, M. R. (2018). Storm protection service of the Sundarbans mangrove forest, Bangladesh. *Natural Hazards*, *94*(1), 405–418. https://doi.org/10.1007/s11069-018-3395-8

Akhter, M., Iqbal, Z., & Chowdhury, R. M. (2008). ASTER imagery of forest areas of Sundarban damaged by cyclone Sidr. *ISME/GLOMIS Electronic Journal*, *6*(1), 5–7.

Alam, E., & Dominey-howes, D. (2015). A new catalogue of tropical cyclones of the northern Bay of Bengal and the distribution and effects of selected landfalling events in Bangladesh. *International Journal of Climatology*, *35*, 801–835. https://doi.org/10.1002/joc.4035

Alongi, D. M. (2009). *The Energetics of Mangrove Forests* (First). Springer Netherlands. https://doi.org/10.1109/ICC.2007.954

Asbridge, E., Lucas, R., Rogers, K., & Accad, A. (2018). The extent of mangrove change and potential for recovery following severe Tropical Cyclone Yasi, Hinchinbrook Island, Queensland, Australia. *Ecology and Evolution*, *8*(21), 10416–10434. https://doi.org/10.1002/ece3.4485

Assal, T. J., Anderson, P. J., & Sibold, J. (2016). Spatial and temporal trends of drought effects in a heterogeneous semi-arid forest ecosystem. *Forest Ecology and Management*, *365*, 137–151. https://doi.org/10.1016/j.foreco.2016.01.017

Assal, T. J., Sibold, J., & Reich, R. (2014). Modeling a Historical Mountain Pine Beetle Outbreak Using Landsat MSS and Multiple Lines of Evidence. *Remote Sensing of Environment, 155*, 275–288. https://doi.org/10.1016/j.rse.2014.09.002

Assal, T. J., Steen, V. A., Caltrider, T., Cundy, T., Stewart, C., Manning, N., & Anderson, P. J. (2021). Monitoring long-term riparian vegetation trends to inform local habitat management in a mountainous environment. *Ecological Indicators, 127*, 107807. https://doi.org/10.1016/j.ecolind.2021.107807

Awty-Carroll, K., Bunting, P., Hardy, A., & Bell, G. (2019). Using continuous change detection and classification of landsat data to investigate long-term mangrove dynamics in the Sundarbans region. *Remote Sensing*, *11*(23), 1–21. https://doi.org/10.3390/rs11232833

Azad, A. S. M. A. Al, Mita, K. S., Zaman, W., & Akter, M. (2018). Impact of Tidal Phase on Inundation and Thrust Force Due to Storm Surge. *Journal of Marine Science and Engineering*, *6*(110). https://doi.org/10.3390/jmse6040110

Aziz, A., & Paul, A. R. (2015). Bangladesh Sundarbans: Present status of the Environment and Biota. *Diversity*, *7*(3), 242–269. https://doi.org/10.3390/d7030242

Bandyopadhyay, S., Dasgupta, S., Khan, Z. H., & Wheeler, D. (2018). *Cyclonic Storm Landfalls in Bangladesh, West Bengal and Odisha, 1877-2016: A Spatiotemporal Analysis* (WPS 8316; Policy Research Working Paper, Issue January).

Barbier, E. B., Koch, E. W., Silliman, B. R., Hacker, S. D., Wolanski, E., Primavera, J., Granek, E. F., Polasky, S., Aswani, S., Cramer, L. A., Stoms, D. M., Kennedy, C. J., Bael, D., Kappel, C. V., Perillo, G. M. E., & Reed, D. J. (2008). Coastal ecosystem-based management with nonlinear ecological functions and values. *Science*, *319*(5861), 321–323. https://doi.org/10.1126/science.1150349

Battisti, C., Poeta, G., & Fanelli, G. (2016). *An Introduction to Disturbance Ecology: A Road Map for Wildlife Management and Conservation* (U. Forstner, W. H. Rulkens, & W. Salomons, Eds.). Springer Nature. https://doi.org/10.1007/978-3-319-32476-0_3

BBC. (2019). *Cyclone Bulbul makes landfall amid India and Bangladesh evacuations—BBC News*. https://www.bbc.com/news/world-asia-50358663

Bhowmik, A., & Cabral, P. (2011). Damage and post-cyclone regeneration assessment of the Sundarbans botanic biodiversity caused by the Cyclone Sidr. *Sustainability, 3*. https://doi.org/10.3390/su30x000x

BMD. (2017). *Historical Cyclones* [PDF]. Bangladesh Meteorological Department (BMD). http://live.bmd.gov.bd/p/Historical-Cyclones/

Chander, G., Markham, B. L., & Helder, D. L. (2009). Summary of current radiometric calibration coefficients for Landsat MSS, TM, ETM+, and EO-1 ALI sensors. *Remote Sensing of Environment*, *113*(5), 893–903. https://doi.org/10.1016/j.rse.2009.01.007

Charrua, A. B., Padmanaban, R., Cabral, P., Bandeira, S., & Romeiras, M. M. (2021). Impacts of the Tropical Cyclone Idai in Mozambique: A Multi-Temporal Landsat Satellite Imagery Analysis. *Remote Sensing*, *13*(2), 201. https://doi.org/10.3390/rs13020201

Cleland, E. E., Chuine, I., Menzel, A., Mooney, H. A., & Schwartz, M. D. (2007). *Shifting plant phenology in response to global change*. *22*(7). https://doi.org/10.1016/j.tree.2007.04.003

Danielsen, F., Sørensen, M. K., Olwig, M. F., Selvam, V., Parish, F., Burgess, N. D., Hiraishi, T., Karunagaran, V. M., Rasmussen, M. S., Hansen, L. B., Quarto, A., & Suryadiputra, N. (2005). The Asian tsunami: A protective role for coastal vegetation. *Science*, *310*(5748), 643. https://doi.org/10.1126/science.1118387

Das, S., & Crépin, A. S. (2013). Mangroves can provide protection against wind damage during storms. *Estuarine, Coastal and Shelf Science*, *134*(October 1999), 98–107. https://doi.org/10.1016/j.ecss.2013.09.021

Das, S., & Vincent, J. R. (2009). Mangroves protected villages and reduced death toll during Indian super cyclone. *Proceedings of the National Academy of Sciences of the United States of America*, *106*(18), 7357–7360. https://doi.org/10.1073/pnas.0810440106

Dasgupta, S., Islam, M. S., Huq, M., Khan, Z. H., & Hasib, M. R. (2019). Quantifying the protective capacity of mangroves from storm surges in coastal Bangladesh. *PLoS ONE*, *14*(3), 1–14. https://doi.org/10.1371/journal.pone.0214079

Dasgupta, S., Islam, Md. S., Huq, M., Khan, Z. H., & Hasib, Md. R. (2017). *Mangroves as Protection from Storm Surges in Bangladesh* (No. 8251; Issue November).

Deb, M., & Ferreira, C. M. (2017). Potential impacts of the Sunderban mangrove degradation on future coastal flooding in Bangladesh. *Journal of Hydro-Environment Research*, *17*, 30–46. https://doi.org/10.1016/j.jher.2016.11.005

del Río-Mena, T., Willemen, L., Vrieling, A., & Nelson, A. (2020). Understanding intra-annual dynamics of ecosystem services using satellite image time series. *Remote Sensing*, *12*(4). https://doi.org/10.3390/rs12040710

Desclée, B., Bogaert, P., & Defourny, P. (2006). Forest change detection by statistical object-based method. *Remote Sensing of Environment*, *102*(1–2), 1–11. https://doi.org/10.1016/j.rse.2006.01.013

DeVries, B., Verbesselt, J., Kooistra, L., & Herold, M. (2015). Robust monitoring of small-scale forest disturbances in a tropical montane forest using Landsat time series. *Remote Sensing of Environment*, *161*, 107–121. https://doi.org/10.1016/j.rse.2015.02.012

Dutta, D., Das, P. K., Paul, S., Sharma, J. R., & Dadhwal, V. K. (2015). Assessment of ecological disturbance in the mangrove forest of Sundarbans caused by cyclones using MODIS time-series data (2001–2011). *Natural Hazards*, *79*(2), 775–790. https://doi.org/10.1007/s11069-015-1872-x

Everitt, A. J. H., Yang, C., Sriharan, S., Judd, F. W., Beach, W. P., Everitt, J. H., Yang, C., Sriharan, S., & Judd, F. W. (2008). Using High Resolution Satellite Imagery to Map Black Mangrove on the Texas Gulf Coast. *Journal of Coastal Research*, *24*(6), 1582–1586. https://doi.org/10.2112/07-0987.1

Field, C. D. (1995). Impact of expected climate change on mangroves. *Hydrobiologia*, *295*, 75–81.

Finkl, C. W., & Makowski, C. (Eds.). (2019). *Encyclopedia of Coastal Science* (Second). Springer. https://doi.org/10.1007/978-3-319-93806-6

Fuller, D. O., & Wdowinski, S. (2007). Mapping Tropical Cyclone Damage to Mangrove Habitats: An Example from South Florida. *AGU Fall Meeting Abstracts*, *1*.

Ghosh, M. K., Kumar, L., & Roy, C. (2017). Climate Variability and Mangrove Cover Dynamics at Species Level in the Sundarbans , Bangladesh. *Sustainability*, *9*(805), 1–16. https://doi.org/10.3390/su9050805

Gilman, E. L., Ellison, J., Duke, N. C., & Field, C. (2008). Threats to mangroves from climate change and adaptation options: A review. *Aquatic Botany*, *89*, 237–250. https://doi.org/10.1016/j.aquabot.2007.12.009

Giri, C., Long, J., Abbas, S., Murali, R. M., Qamer, F. M., Pengra, B., & Thau, D. (2015). Distribution and dynamics of mangrove forests of South Asia. *Journal of Environmental Management*, *148*, 101–111. https://doi.org/10.1016/j.jenvman.2014.01.020

Giri, C., Ochieng, E., Tieszen, L. L., Zhu, Z., Singh, A., Loveland, T., Masek, J., & Duke, N. (2011). Status and distribution of mangrove forests of the world using earth observation satellite data. *Global Ecology and Biogeography*, *20*(1), 154–159. https://doi.org/10.1111/j.1466-8238.2010.00584.x

Giri, C., Pengra, B., Zhu, Z., Singh, A., & Tieszen, L. L. (2007). Monitoring mangrove forest dynamics of the Sundarbans in Bangladesh and India using multi-temporal satellite data from 1973 to 2000. *Estuarine, Coastal and Shelf Science*, *73*(1–2), 91–100. https://doi.org/10.1016/j.ecss.2006.12.019

Hardisky, M. A., Daiber, F. C., Roman, C. T., & Klemas, V. (1984). Remote sensing of biomass and annual net aerial primary productivity of a salt marsh. *Remote Sensing of Environment*, *16*(2), 91–106. https://doi.org/10.1016/0034-4257(84)90055-5

Hiraishi, T., & Harada, K. (2003). *Green Belt Tsunami Prevention in South-Pacific Region*.

Hobbs, R. J., & Huenneke, L. F. (1992). Disturbance, Diversity, and Invasion: Implications for Conservation. *Conservation Biology*, *6*(3), 324–337. https://doi.org/10.1046/j.1523-1739.1992.06030324.x

Hogarth, P. J. (2015). The Biology of Mangroves and Seagrasses. In *Biology of Habitats* (Third). Oxford University Press.

Hoque, A. K. F., & Datta, D. K. (2005). The mangroves of Bangladesh. *International Journal of Ecology and Environmental Sciences*, *31*(3), 245–253.

Hoque, M. A. A., Phinn, S., Roelfsema, C., & Childs, I. (2016). Assessing tropical cyclone impacts using object-based moderate spatial resolution image analysis: A case study in Bangladesh. *International Journal of Remote Sensing*, *37*(22), 5320–5343. https://doi.org/10.1080/01431161.2016.1239286

Hussain, M., Chen, D., Cheng, A., Wei, H., & Stanley, D. (2013). Change detection from remotely sensed images: From pixel-based to object-based approaches. *ISPRS Journal of Photogrammetry and Remote Sensing*, *80*, 91–106. https://doi.org/10.1016/j.isprsjprs.2013.03.006

Im, J., Jensen, J. R., & Tullis, J. A. (2013). Object-based change detection using correlation image analysis and image segmentation. *International Journal of Remote Sensing*, *29*(2), 399–423. https://doi.org/10.1080/01431160601075582

Islam, M. M., Borgqvist, H., & Kumar, L. (2019). Monitoring Mangrove forest landcover changes in the coastline of Bangladesh from 1976 to 2015. *Geocarto International*, *34*(13), 1458–1476. https://doi.org/10.1080/10106049.2018.1489423

Janzen, D. H. (1985). Mangroves: Where ' s the understory? Mangroves: Where ' s the understory ? *Journal of Tropical Ecology*, *1*(1), 89–92. https://doi.org/10.1017/S0266467400000122

Johansen, K., Arroyo, L. A., Phinn, S., & Witte, C. (2010). Comparison of geo-object based and pixel-based change detection of riparian environments using high spatial resolution multi-spectral imagery. *Photogrammetric Engineering and Remote Sensing*, *76*(2), 123–136. https://doi.org/10.14358/PERS.76.2.123

Joshi, N., Baumann, M., Ehammer, A., Fensholt, R., Grogan, K., Hostert, P., Jepsen, M. R., Kuemmerle, T., Meyfroidt, P., Mitchard, E. T. A., Reiche, J., Ryan, C. M., & Waske, B. (2016). A review of the application of optical and radar remote sensing data fusion to land use mapping and monitoring. *Remote Sensing*, *8*(1), 1–23. https://doi.org/10.3390/rs8010070

Kamthonkiat, D., Rodfai, C., Saiwanrungkul, A., Koshimura, S., & Matsuoka, M. (2011). Geoinformatics in mangrove monitoring: Damage and recovery after the 2004 Indian Ocean tsunami in Phang Nga, Thailand. *Natural Hazards and Earth System Science*, *11*(7), 1851–1862. https://doi.org/10.5194/nhess-11-1851-2011

Kanniah, K. D., Sheikhi, A., Cracknell, A. P., Goh, H. C., Tan, K. P., Ho, C. S., & Rasli, F. N. (2015). Satellite images for monitoring mangrove cover changes in a fast growing economic region in southern Peninsular Malaysia. *Remote Sensing*, *7*(11), 14360–14385. https://doi.org/10.3390/rs71114360

Kathiresan, K., & Rajendran, N. (2005). Coastal mangrove forests mitigated tsunami. *Estuarine, Coastal and Shelf Science*, *65*(3), 601–606. https://doi.org/10.1016/j.ecss.2005.06.022

Kennedy, R. E., Yang, Z., & Cohen, W. B. (2010). Detecting trends in forest disturbance and recovery using yearly Landsat time series: 1. LandTrendr — Temporal segmentation algorithms. *Remote Sensing of Environment*, *114*(12), 2897–2910. https://doi.org/10.1016/j.rse.2010.07.008

Knutson, T. R., McBride, J. L., Chan, J., Emanuel, K., Holland, G., Landsea, C., Held, I., Kossin, J. P., Srivastava, A. K., & Sugi, M. (2010). Tropical cyclones and climate change. *Nature Geoscience*, *3*(3), 157–163. https://doi.org/10.1038/ngeo779

Krauss, K. W., & Osland, M. J. (2020). Tropical cyclones and the organization of mangrove forests: A review. *Annals of Botany*, *125*(2), 213–234. https://doi.org/10.1093/aob/mcz161

Krebs, C. J. (2014). *Ecology: Pearson New International Edition: The Experimental Analysis of Distribution and Abundance* (Sixth, Vol. 56, Issue 4). Pearson.

Kumar, S., Lal, P., & Kumar, A. (2020). Turbulence of tropical cyclone ‘ Fani ’ in the Bay of Bengal and Indian subcontinent. *Natural Hazards*, *103*, 1613–1622. https://doi.org/10.1007/s11069-020-04033-5

Lewis, A. J., & MacDonald, H. C. (1972). Mapping of mangrove and perpendicular-oriented shell reefs in southeastern panama with side-looking radar. *Photogrammetria*, *28*, 187–199.

Long, J., Giri, C., Primavera, J., & Trivedi, M. (2016). Damage and recovery assessment of the Philippines’ mangroves following Super Typhoon Haiyan. *Marine Pollution Bulletin*, *109*(2), 734–743. https://doi.org/10.1016/j.marpolbul.2016.06.080

Lu, D., Mausel, P., Brondízio, E., & Moran, E. (2004). Change detection techniques. *International Journal of Remote Sensing*, *25*(12), 2365–2401. https://doi.org/10.1080/0143116031000139863

Macamo, C. C. F., Massuanganhe, E., Nicolau, D. K., Bandeira, S. O., & Adams, J. B. (2016). Mangrove’s response to cyclone Eline (2000): What is happening 14 years later. *Aquatic Botany*, *134*, 10–17. https://doi.org/10.1016/j.aquabot.2016.05.004

Marois, D. E., & Mitsch, W. J. (2015). Coastal protection from tsunamis and cyclones provided by mangrove wetlands—A review. *International Journal of Biodiversity Science, Ecosystem Services and Management*, *11*(1), 71–83. https://doi.org/10.1080/21513732.2014.997292

Mazda, Y., Magi, M., Kogo, M., & Phan Nguyen Hong. (1997). Mangroves as a coastal protection from waves in the Tong King Delta, Vietnam. In *Mangroves and Salt Marshes* (Vol. 1, Issue 2, pp. 127–135). Kluwer Academic Publishers. https://doi.org/10.1023/A:1009928003700

McAdie, C. J., Landsea, C. W., Neumann, C. J., David, J. E., Blake, E. S., & Hammer, G. R. (2009). Tropical Cyclones of the North Atlantic Ocean 1851-2006. In *Historical Climatology Series* (Vol. 6, Issue 2).

MFDM. (2008). *SUPER CYCLONE SIDR 2007 Impacts and Strategies for Interventions*.

Mitchell, A. L., Rosenqvist, A., & Mora, B. (2017). Current remote sensing approaches to monitoring forest degradation in support of countries measurement, reporting and verification (MRV) systems for REDD+. In *Carbon Balance and Management* (Vol. 12, Issue 9). BioMed Central Ltd. https://doi.org/10.1186/s13021-017-0078-9

Njoku, E. G. (Ed.). (2014). Encyclopedia of Remote Sensing. In *Encyclopedia of Remote Sensing*. Springer. https://doi.org/10.1007/978-0-387-36699-9

Pasetto, D., Arenas-Castro, S., Bustamante, J., Casagrandi, R., Chrysoulakis, N., Cord, A. F., Dittrich, A., Domingo-Marimon, C., El Serafy, G., Karnieli, A., Kordelas, G. A., Manakos, I., Mari, L., Monteiro, A., Palazzi, E., Poursanidis, D., Rinaldo, A., Terzago, S., Ziemba, A., & Ziv, G. (2018). Integration of satellite remote sensing data in ecosystem modelling at local scales: Practices and trends. *Methods in Ecology and Evolution*, *9*(8), 1810–1821. https://doi.org/10.1111/2041-210X.13018

Pastor-Guzman, J., Dash, J., & Atkinson, P. M. (2018). Remote sensing of mangrove forest phenology and its environmental drivers. *Remote Sensing of Environment*, *205*(January 2017), 71–84. https://doi.org/10.1016/j.rse.2017.11.009

Peters, D. P. C., Lugo, A. E., Chapin, F. S., Pickett, S. T. A., Duniway, M., Rocha, A. V., Swanson, F. J., Laney, C., & Jones, J. (2011). Cross-system comparisons elucidate disturbance complexities and generalities. *Ecosphere*, *2*(7), 1–26. https://doi.org/10.1890/ES11-00115.1

Pettorelli, N., Vik, J. O., Mysterud, A., Gaillard, J. M., Tucker, C. J., & Stenseth, N. C. (2005). Using the satellite-derived NDVI to assess ecological responses to environmental change. *Trends in Ecology and Evolution*, *20*(9), 503–510. https://doi.org/10.1016/j.tree.2005.05.011

Pickett, S. T. A., & White, P. S. (Eds.). (1985). *The Ecology of Natural Disturbance and Patch Dynamics*. Academic Press. https://doi.org/10.2307/5048

Quader, M. A., Agrawal, S., & Kervyn, M. (2017). Multi-decadal land cover evolution in the Sundarban, the largest mangrove forest in the world. *Ocean and Coastal Management*, *139*(October), 113–124. https://doi.org/10.1016/j.ocecoaman.2017.02.008

R Development Core Team. (2013). R: A language and environment for statistical computing.

Reef, R., Feller, I. C., & Lovelock, C. E. (2010). Nutrition of mangroves. *Tree Physiology*, *30*(9), 1148–1160. https://doi.org/10.1093/treephys/tpq048

Reliefweb. (2007). *Bangladesh: Life-saving Sundarbans may take years to recover from cyclone—Bangladesh | ReliefWeb*. ReliefWeb. https://reliefweb.int/report/bangladesh/bangladesh-life-saving-sundarbans-may-take-years-recover-cyclone

Richardson, A. D., Keenan, T. F., Migliavacca, M., Ryu, Y., Sonnentag, O., & Toomey, M. (2013). Agricultural and Forest Meteorology Climate change , phenology , and phenological control of vegetation feedbacks to the climate system. *Agricultural and Forest Meteorology*, *169*, 156–173. https://doi.org/10.1016/j.agrformet.2012.09.012

Rouse, J. W., Haas, R. H., Deering, D. W., Schell, J. A., & Harlan, J. C. (1974). *MONITORING THE VERNAL ADVANCEMENT AND RETROGRADATION (GREENWAVE EFFECT) OF NATURAL VEGETATION*.

Sahoo, B., & Bhaskaran, P. K. (2016). Assessment on historical cyclone tracks in the Bay of Bengal, east coast of India. *International Journal of Climatology*, *36*(1), 95–109. https://doi.org/10.1002/joc.4331

Sandilyan, S., & Kathiresan, K. (2012). Mangrove conservation: A global perspective. *Biodiversity and Conservation*, *21*(14), 3523–3542. https://doi.org/10.1007/s10531-012-0388-x

Sandilyan, S., & Kathiresan, K. (2015). Mangroves as bioshield: An undisputable fact. *Ocean and Coastal Management*, *103*(January 2012), 94–96. https://doi.org/10.1016/j.ocecoaman.2014.11.011

Sanford, M. P. (2009). Valuating Mangrove Ecosystems as Coastal Protection in Post-Tsunami South Asia. *Natural Areas*, *29*(1), 91–95.

Sippo, J. Z., Lovelock, C. E., Santos, I. R., Sanders, C. J., & Maher, D. T. (2018). Mangrove mortality in a changing climate: An overview. *Estuarine, Coastal and Shelf Science*, *215*, 241–249. https://doi.org/10.1016/j.ecss.2018.10.011

Small, C., & Sousa, D. (2019). Spatiotemporal characterization of mangrove phenology and disturbance response: The Bangladesh Sundarban. *Remote Sensing*, *11*(17). https://doi.org/10.3390/rs11172063

Songsom, V., Koedsin, W., Ritchie, R. J., & Huete, A. (2019). Mangrove phenology and environmental drivers derived from remote sensing in Southern Thailand. *Remote Sensing*, *11*(8). https://doi.org/10.3390/rs11080928

Spalding, M., Blasco, F., & Field, C. (Eds.). (1997). *World mangrove atlas* (First). The International Society for Mangrove Ecosystems.

Szpakowski, D. M., & Jensen, J. L. R. (2019). A Review of the Applications of Remote Sensing in Fire Ecology. *Remote Sensing*, *11*(22). https://doi.org/10.1007/978-3-319-51727-8_254-1

Toomey, M., Roberts, D. A., Still, C., Goulden, M. L., & McFadden, J. P. (2011). Remotely sensed heat anomalies linked with Amazonian forest biomass declines. *Geophysical Research Letters*, *38*(19), 1–5. https://doi.org/10.1029/2011GL049041

UNESCO. (2007). *Sundarbans World Heritage site devastated by cyclone, according to UNESCO experts who visited the site*. https://whc.unesco.org/en/news/399

Wang, L., Jia, M., Yin, D., & Tian, J. (2019). A review of remote sensing for mangrove forests: 1956–2018. *Remote Sensing of Environment*, *231*. https://doi.org/10.1016/j.rse.2019.111223

Wang, L., & Qu, J. J. (2007). NMDI : A normalized multi-band drought index for monitoring soil and vegetation moisture with satellite remote sensing. *Geophysical Research Letters*, *34*(20), 1–5. https://doi.org/10.1029/2007GL031021

Wang, T., Zhang, H., Lin, H., & Fang, C. (2016). Textural-spectral feature-based species classification of mangroves in Mai Po nature reserve from worldview-3 imagery. *Remote Sensing*, *8*(1), 1–15. https://doi.org/10.3390/rs8010024

Wang, W., Qu, J. J., Hao, X., Liu, Y., & Stanturf, J. A. (2010). Post-hurricane forest damage assessment using satellite remote sensing. *Agricultural and Forest Meteorology*, *150*(1), 122–132. https://doi.org/10.1016/j.agrformet.2009.09.009

Wilson, E. H., & Sader, S. A. (2002). Detection of forest harvest type using multiple dates of Landsat TM imagery. *Remote Sensing of Environment*, *80*(3), 385–396. https://doi.org/10.1016/S0034-4257(01)00318-2

Xue, J., & Su, B. (2017). Significant Remote Sensing Vegetation Indices: A Review of Developments and Applications. *Journal of Sensors, 2017*.

Zhang, K., Thapa, B., Ross, M., & Gann, D. (2016). Remote sensing of seasonal changes and disturbances in mangrove forest: A case study from South Florida. *Ecosphere, 7*(6), 1–23. https://doi.org/10.1002/ecs2.1366

Zhu, Z., Woodcock, C. E., & Olofsson, P. (2012). Continuous monitoring of forest disturbance using all available Landsat imagery. *Remote Sensing of Environment, 122*, 75–91. https://doi.org/10.1016/j.rse.2011.10.030

APPENDIX

Purpose: This script will create mean NDVI from MODIS (MOD09Q1.006 Terra Surface Reflectance 8-Day Global 250m) based on a specific period. It takes one year at a time into consideration to provide the images and perform the analysis. It will calculate the NDVI from the collection and apply a minimum observation filter to ensure the consistency of the image collection. Later, it will calculate the monthly mean NDVI and export the images to the commanded drive location. Further analysis will be done in R Studio using those outputs.

Image Collection Used: MOD09Q1.006 Terra Surface Reflectance 8-Day Global 250m

```
/////   NDVI Monthly Stats Calculation for SB Area using MODIS 8-Day 250m   /////

/*

STEPS:

  //establishes sets of dates and start/end months/years

  //masks the MODIS daily surface reflectance (250m resolution) collection

  //calculates NDVI

  //applies the minimum observation filter on a monthly level

  //calculates local monthly means for the selected dates

  //exports each month as its own image using a client-side for-loop

*/

/////// PART 1A: CREATE IMAGE COLLECTION ///////
```

```
// filter m250sr collection by years of study

//uncomment to run the script in sets - change to smaller interval if needed

var startdate =ee.Date(

  '2010-01-01' //test set

  )

var enddate = ee.Date(

  '2010-12-31' // test set

  )

var startmonth = startdate.get('month')

var startyear = startdate.get('year')

var endmonth = enddate.get('month')

var endyear = enddate.get('year')

//filter daily sr 250 collections to specific dates

var m250 = ee.ImageCollection(m250_8day_sr)

  .filter(ee.Filter.calendarRange(startyear, endyear,'year'))

  .filter(ee.Filter.calendarRange(startmonth, endmonth,'month'))

print(m250)
```

```
/////// PART 1B: MASKING IMAGE COLLECTION  ///////

// write fxn to get the Bit Information from QA Band

var single = ee.Image(m250.first())

var getQABits = function(single, start, end, newName) {

  // Compute the bits we need to extract.

  var pattern = 0;

  for (var i = start; i <= end; i++) {

    pattern += Math.pow(2, i);

  }

  return single.select([0], [newName])

                .bitwiseAnd(pattern)

                .rightShift(start);

};

// CREATE BIT VARIABLES  //

// Select the QA band

var QA = single.select('State')

// Get various bits from the 'State' band

var land_water = getQABits(QA, 3, 5, 'land_water_flag')
```

```
.expression("b(0)!=0 && b(0)!=1"); //1= land, 3= shallow inland water

var cloud_all = getQABits(QA, 0, 1, 'cloud_state')

.expression("b(0)!=0 && b(0)!=3");//0= clear, 3= Not set, assumed clear

// Create a mask that filters out shallow & deep inland water and cloudy areas.

var mask_m250_8day = function(image) {

  var mask = land_water.neq(3).neq(5).and(cloud_all.not()) //3=shallow inland water, 5= deep
inland water

  return ee.Image(image).updateMask(mask)

};

// call masking fxn - apply to image collection

var m250_masked = m250.map(mask_m250_8day)

print('m250_masked', m250_masked)

/////// PART 1C: Calculate NDVI of each pixel of each image ///////

// BAND CALC //

//define function to add an NDVI band

var addNDVI = function(image){

  var ndvi = image.normalizedDifference(['sur_refl_b02', 'sur_refl_b01']).rename('NDVI');

  return image.addBands(ndvi);

};
```

```
var m250ndvi = m250_masked.map(addNDVI);

print('m250ndvi ex image',m250ndvi.first());

print('m250ndvi.proj',m250ndvi.first().projection())

/////// PART 3: APPLY VALID PIXEL & MINOBS FILTERS ///////

// 3A: CALCULATE NUMBER OF VALID OBSERVATIONS FROM PIXEL IN A GIVEN TIME SERIES //

// Define month and year range variables

var months = ee.List.sequence(startmonth, endmonth);

var years = ee.List.sequence(startyear, endyear);

// Define a function to calculate the number of valid observations for a given pixel's time series.

// Counts number of times a pixel is valid across each unique month (each month of each year)

//result is image collection with rasters counting each time each pixel was masked for each unique month

var valPixCountColl = ee.ImageCollection.fromImages(

  years.map(function(y){

    return months.map(function(m){

        var time = ee.Date.fromYMD(y,m,1) //take the year, month, and 1st day

        var custom_time = ee.Number.parse(time.format('YYYYMM'))

    return m250ndvi //replaced m250Set w m250ndvi on 1/11
```

```
        .filter(ee.Filter.calendarRange(y, y, 'year'))
        .filter(ee.Filter.calendarRange(m, m, 'month'))
        //validPixelCount function
        .map(function(img) {
                return img.select(0).mask();
               }).sum().selfMask().clip(AOI)
        //set timestamps
        .set('month', m).set('year', y)
        .set('system:time_start', time.millis())
        .set('custom:time_start', custom_time)
}).flatten()
  }).flatten())
print('valPixCountColl', valPixCountColl);
var validPixelCountViz =  {min: 1, max: 30};
Map.addLayer(valPixCountColl, validPixelCountViz, 'ValidPixelCount');
// 3B: SET MINIMUM NUMBER OF CLEAR OBSERVATIONS //
// DEFINE THRESHOLD //
// Reclassify observations by threshold (e.g., min 5 clear obs)
```

```
// Define the threshold value, the minimum number of times a pixel has to be valid to be used in the mean at all

var thresh = 4; //NOTE: we can use the thresh in the monthly calculation, since we know how many days there will be per month

//make observation threshold calculation into a function

var obsThreshGen = function(image){

  return image

        .gte(thresh)

        .remap([1], [1], null)

        .rename('ObsThreshold')

        //preserve time stamps //idea: might just use a "copy metadata" function? the current way works, but looks clunky

        .set('system:time_start', image.get('system:time_start'))

        .set('custom:time_start', ee.String(image.get('custom:time_start')))

        .set('month', image.get('month'))

        .set('year', image.get('year'))

        .set('system:index', image.get('system:index'))

}
```

```
//Create an obsThreshold for each month in the collection

// result should be an image collection with an element for each unique local month

var ObsThreshColl = valPixCountColl.map(obsThreshGen)

//ObsThreshColl is a collection with each image having a unique observation threshold raster or
1's and null values

print ('ObsThreshColl', ObsThreshColl);

//Map.addLayer(ObsThreshColl);

//give each image in the collection a month and year stamp

var addMY = function(img){

      //define variables for each month and year for custom date

      var mon =  ee.Date(img.get('system:time_start')).format('MM')

      var mon_num = ee.Number(mon)

      var yr = ee.Date(img.get('system:time_start')).format('YYYY')

      var yr_num = ee.Number(yr)

      var MY_date = ee.String(yr_num).cat(mon_num)

   return img  //give it a timestamp

      .set('month', mon_num)

      .set('year', yr_num)

      .set('custom:time_start', MY_date)
```

```
        .set('system:time_start', img.get('system:time_start'))

        }

var m250Set_MY = m250ndvi.map(addMY) //replace m250Set with m250ndvi on 1/11

print('m250Set_MY', m250Set_MY.first())

//join image collecion to obsThresh monthly filter

var inJoin = ee.Join.inner()

var filterByMY = ee.Filter.equals({

  leftField: 'custom:time_start',

  rightField: 'custom:time_start'

});

//apply join to the daily image and monthy obsThreshold Collections

var m250_MYThresh = inJoin.apply(ObsThreshColl, m250Set_MY, filterByMY);

print("m250_MYThresh", m250_MYThresh.first())

// create a function to merge the bands together after a join

// result should be an image collection of nyears*nmonths

var mergeBands = function(row){

  var image = ee.Image.cat(row.get('primary'), row.get('secondary'))

  return image;
```

```
};

var MYThresh_DS = m250_MYThresh.map(mergeBands)

print("MYThresh_DS", MYThresh_DS)

var m250_MYT = ee.ImageCollection(MYThresh_DS)

//define minObs calculation function

var minObsCalc = function(img){

  var expr = img.expression('NDVI*ObsThreshold',{

                'NDVI': img.select('NDVI'),

                'ObsThreshold': img.select('ObsThreshold')}).rename('NDVI_mo') //mo = MinObs

  return img.addBands(expr).copyProperties(img)

}

//call minObs fxn to new dataset MYT (MonthYearThresh)

var m250_minObs = m250_MYT.map(minObsCalc).select('NDVI_mo') //mo = MinObs

print('m250_minObs', m250_minObs)

//Map.addLayer(m250_minObs)

//var m250_MR = m250_minObs.map(multMR)

//print('m250_MR', m250_MR)
```

```
/////// PART 4: CALCULATE LOCAL MONTHLY MEANS ///////

//result should be a collection with nyears * nmonths (2 full years of data = 24 elements)

// calulates local monthly means (first filter annually, then monthly, then calc the mean)

var byMonthYear = ee.ImageCollection.fromImages(

  years.map(function(y){ //for each year 'y'

    return months.map(function (m){ //for each month 'm' of year 'y'

        var time = ee.Date.fromYMD(y,m,1) //take the year, month, and 1st day

        var custom_time = ee.Number.parse(time.format('YYYYMM'))  //set this to the year and month (eg 2017_02)

      return m250_minObs //for each month of each year, take this image set and...

        .filter(ee.Filter.calendarRange(y, y, 'year'))

        .filter(ee.Filter.calendarRange(m, m, 'month'))

        .select("NDVI_mo").mean().rename("NDVI_mmean") // mmean = 'Monthly Mean'

        .set('month', m).set('year', y) //set a month and year variable

        .set('system:time_start', time.millis()) //give it a timestamp

        .set(ee.String('custom:time_start'), custom_time) //give it a user-readable YYYY_MM stamp

        //.addBands(ee.Image(custom_time).rename('time'));

    });
```

```
  }).flatten() //take the collection of collections and flatten
  );
print('byMonthYear', byMonthYear)
//multiply by 10,000 then turn to Int16 form (no decimals) to save time and shrink total data size
on export
var shrink = function(img){
  var scaleUp =
img.select('NDVI_mmean').multiply(ee.Number(10000)).rename('NDVI_mm_scaledUp')
  return img.addBands(scaleUp).select('NDVI_mm_scaledUp').toInt16()
}
//apply "shrink" fxn to change to Int16
var BMY_Int16 = byMonthYear.map(shrink)
print(BMY_Int16)
var BMY_Int16_month = BMY_Int16.filter(ee.Filter.equals('month', 01)).first().clip(AOI)
Map.addLayer(BMY_Int16_month)
//add first image from both float and int to map to compare values
//Map.addLayer(byMonthYear.first(), {bands: 'NDVI_mmean'}, 'localMean_float')
//Map.addLayer(BMY_Int16.first(), {bands: 'NDVI_mm_scaledUp'}, 'localMean_Int16')
```

```
////// PART 5: For-Loop to Export Images ///////

//NOTE: This will run if you give it enough time (I pressed "Wait" twice when prompted)

//change commented variable if changing the data type

//byMonthYear is float data type, BMY_Int16 is integer 16

// create var for the size of the total image collection w each local means

var size =

//byMonthYear

BMY_Int16

.size().getInfo()

// create a list of these images, as large as the # of local mean images ("size")

var BMY_list =

//byMonthYear

BMY_Int16

.toList(size)

var size =

//byMonthYear

valPixCountColl

.size().getInfo()
```

```
// create a list of these images, as large as the # of local mean images ("size")
var valPixCount_list =
//byMonthYear
valPixCountColl
.toList(size)
//export each image with the date as the file name
//keeps going as long as n < size (i.e. go through the entire list)
/*
//note: need for-loop instead of .map(); export is a client-side function
for (var n=0; n<size; n++) {
  var image = ee.Image(BMY_list.get(n)) //first get image 1, then get image 2, etc.
  var date = ee.Date(image.get('system:time_start')).format('YYYY-MM'); //var 'date' used for naming, e.g. '2013-06'
  date = date.getInfo();
  Export.image.toDrive({
    image: image.toFloat().divide(10000), //converted from integer to float and used scale factor of 10000
    description: date,
    fileNamePrefix: date, // this is the file name
```

```
    folder: 'MODIS_NEW', //***NOTE: change to name of desired Drive folder
    scale: 250,
    region: AOI,
    crs: 'EPSG:32646'
    //maxPixels: 130000000000,
  })
}
*/
////////////////////////////////////////////////////
//To map the valid pixels
for (var n=0; n<size; n++) {
  var image = ee.Image(valPixCount_list.get(n)) //first get image 1, then get image 2, etc.
  var date = ee.Date(image.get('system:time_start')).format('YYYY-MM'); //var 'date' used for naming, e.g. '2013-06'
  date = date.getInfo();
  Export.image.toDrive({
    image: image,
    description: date,
    fileNamePrefix: date, // this is the file name
```

```
    folder: 'VPC_MODIS', //***NOTE: change to name of desired Drive folder
    scale: 250,
    region: AOI,
    crs: 'EPSG:32646'
    //maxPixels: 130000000000,
  })
}
```